The aftermath of the CPE and the Carnian–Norian transition in northwestern Sichuan Basin, South China

Xin Jin[1,2]*, Christopher A. McRoberts[3], Zhiqiang Shi[2], Paolo Mietto[1], Manuel Rigo[1], Guido Roghi[4], Stefano Manfrin[1], Marco Franceschi[1] & Nereo Preto[1]

[1] Dipartimento di Geoscienze, Università degli Studi di Padova, Via G. Gradenigo 6, Padova, Italy
[2] State Key Laboratory of Oil and Gas Reservoir Geology and Exploitation, Chengdu University of Technology, Chengdu, Sichuan 610059, China
[3] Department of Geology, State University of New York at Cortland, P.O. Box 2000, Cortland, NY 13045, USA
[4] Istituto di Geoscienze e Georisorse (IGG-CNR), Via G. Gradenigo 6, 35131 Padova, Italy
N.P., 0000-0001-8757-328X
* Correspondence: jinxin2012cdut@163.com

Abstract: The northwestern Sichuan Basin (South China) was a portion of eastern Tethys where, during the Late Triassic, a sharp lithological transition from oolitic–bioclastic limestones and sponge reef mounds to dark grey terrigenous clays, siltstones and sandstones is visible in several localities. The timing and significance of this major facies transition is still unclear. Here we report new biostratigraphic and carbon stable isotope data from Hanwang and Jushui, northwestern Sichuan Basin. Sporomorphs, ammonoids, conodonts and halobiid bivalves show that the lithological change is Late Carnian to Early Norian in age. This amended age determination facilitates recalibration of the magnetostratigraphy in the area allowing correlation between the Late Triassic of the Sichuan Basin and the Astrochronostratigraphic Polarity Time Scale. A carbon stable isotopic perturbation across the Carnian–Norian Boundary (CNB) is missing in our sections, or it is concealed because of the mixed organic matter sources. Our findings pinpoint the position of the CNB to a short stratigraphic interval of *c.* 12 m thickness in the Sichuan Basin. The studied sections greatly extend the palaeogeographical documentation of the CNB and provide novel information on biostratigraphy and chemostratigraphy that should be considered in defining the best position of the Norian Global Stratotype Section and Point.

**Received** 23 May 2018; **revised** 31 October 2018; **accepted** 1 November 2018

At least two main episodes of biotic crisis and environmental change are documented during the Late Triassic, the Carnian Pluvial Episode (CPE) (Simms & Ruffell 1989, 2018) and the end-Triassic mass extinction, which is one of 'big five' mass extinctions in the Phanerozoic (Raup & Sepkoski 1982). Both are associated with major negative δ^{13}C perturbations (carbon isotope excursions; CIEs) (Whiteside *et al.* 2010; Dal Corso *et al.* 2018, and references therein). The CIE at the Carnian Pluvial Episode has been so far documented in a few bulk organic carbon and *n*-alkane records (Dal Corso *et al.* 2012, 2015, 2018; Mueller *et al.* 2015, 2016; Sun *et al.* 2016; Miller *et al.* 2017; Baranyi *et al.* 2018; Shi *et al.* 2018) and also reported in carbonate records (Sun *et al.* 2016, 2018), and the carbon isotopic record of the end-Triassic mass extinction has been extensively studied (e.g. Hesselbo *et al.* 2002; Schoene *et al.* 2010; Whiteside *et al.* 2010). In both cases, the biotic and environmental changes were possibly related to emissions of CO_2 as a consequence of the eruption of a large igneous province (Furin *et al.* 2006; Schoene *et al.* 2010; Whiteside *et al.* 2010; Dal Corso *et al.* 2012, 2015, 2018; Sun *et al.* 2016, 2018).

The stratigraphic interval after the CPE is relatively poorly studied, and the definition of the boundaries between the three Upper Triassic stages (Carnian, Norian and Rhaetian) is still a matter of debate (Lucas 2018). Two main Global Stratotype Section and Point (GSSP) candidate sections of the Carnian–Norian Boundary (CNB) have been proposed and studied for their biostratigraphy and carbon stable isotopic stratigraphy: Black Bear Ridge in British Columbia (e.g. Orchard *et al.* 2001; McRoberts 2007, 2011; Orchard 2007, 2014; Williford *et al.* 2007; Zonneveld *et al.* 2010; Onoue *et al.* 2016) and Pizzo Mondello in Sicily (e.g. Muttoni *et al.* 2001; Nicora *et al.* 2007; Mazza *et al.* 2010, 2012;

2018; Balini *et al.* 2012). Magnetostratigraphy is available from Pizzo Mondello (Muttoni *et al.* 2004), and it has been suggested that the Norian GSSP should be located at the first occurrence (FO) of the conodont *Metapolygnathus parvus* (Mazza *et al.* 2018; Rigo *et al.* 2018). *Halobia* faunas (bivalves) at Pizzo Mondello were studied and correlated to ammonoid biozones by Levera (2012), showing that *Halobia austriaca* is the best halobiid marker for defining the base of the Norian GSSP.

We here document stratigraphic sections that are younger than the Ma'antang section (Shi *et al.* 2018) including the aftermath of the CPE and CNB interval from the Longmen Shan area in the northwestern Sichuan Basin, a region far from the two proposed GSSP localities of Black Bear Ridge and Pizzo Mondello (BBR and PMS in Fig. 1a).

The Sichuan Basin hosts a thick succession of Upper Triassic rocks, from Carnian ramp carbonates to Carnian–Norian marginal marine and continental siliciclastic rocks (Li *et al.* 2003; Wu 2009). Their sequence stratigraphic correlation has been discussed by He *et al.* (2011) and Mei & Liu (2017), mainly combining outcrop with core data. Fragmentary biostratigraphic data include ammonoids and bivalves (Wu 1989; Wang 1992; Shi *et al.* 2017), foraminifera (He 1980), conodonts (Shi *et al.* 2017; Jin *et al.* 2018) and palynofloras (Li & Wang 2016; Li *et al.* 2016, 2017a). The CNB in the area has so far been positioned on the basis of these scarce biostratigraphic data and is still poorly constrained. Recently, Li *et al.* (2017b) investigated the magnetostratigraphy of an overlying siliciclastic succession and constrained its age from Norian to Rhaetian. Zhang *et al.* (2015) and Shi *et al.* (2017) provided magnetostratigraphic and biostratigraphic data from the Qingyan Gou section in the Sichuan Basin and considered the sharp
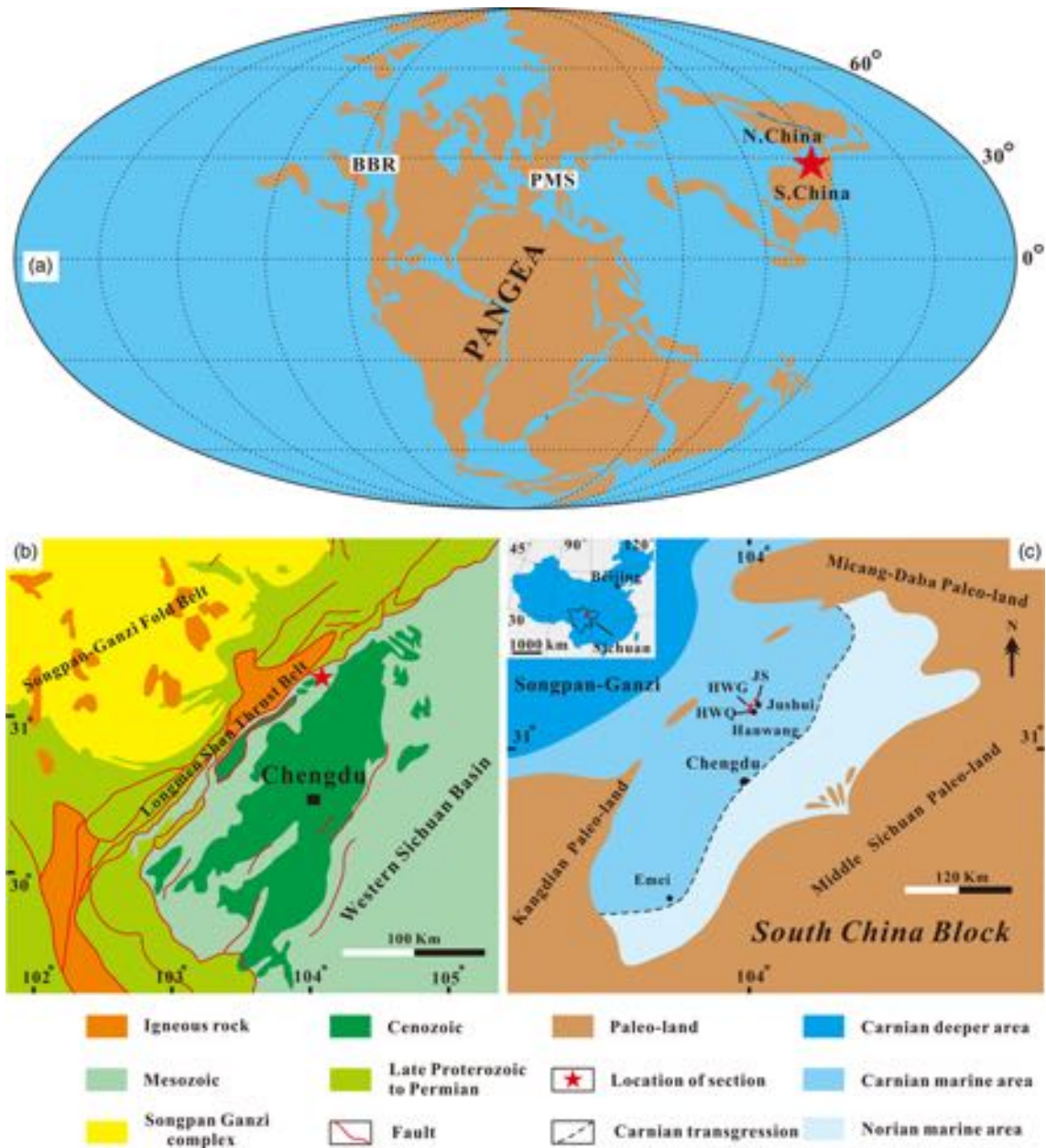
Fig. 1. Location of the study area and sections during the Late Triassic. (**a**) Position of study area (star) in eastern Tethys during the Late Triassic (simplified from Golonka 2007). Carnian–Norian GSSP candidate sections: BBR, Black Bear Ridge, British Columbia; PMS, Pizzo Mondello, Sicily. (**b**) Geological and tectonic map of the Sichuan Basin and adjacent areas (simplified from Shi *et al.* 2017). (**c**) Late Triassic palaeogeography of the western Sichuan Basin and locations of study sections in the Hanwang and Jushui areas (simplified from Wu 1989). HWQ, Qingyan Gou section; HWG, Guanyin Ya section; JS, Jushui section.

lithological transition from carbonates to shales as related to the CPE. However, Jin *et al.* (2018) reported a Tuvalian 3 (late Carnian) conodont association from the carbonate units of the Qingyan Gou section, which would exclude the presence of the CPE.

In an effort to better constrain this stratigraphic interval, new ammonoids, bivalves, conodonts and palynomorphs were collected and determined from the sections considered in this study. Carbon isotopic composition of organic matter (OM) was analysed on bulk-rock and wood, to assess the stable isotope record in this stratigraphic interval in the Sichuan Basin and compare it with that in other regions. Although not coincident with major shifts in the isotope record or major extinction events, the CNB is placed in a time when important biotic changes were occurring; for instance, the major differentiation of conifers (Miller 1982; Renner 2009). Therefore, investigations aimed at better characterizing this interval are needed. Results presented in the present paper go in this

direction and clarify the Upper Triassic stratigraphic framework of the northwestern Sichuan Basin, allowing better correlations with sections in the western Tethys. Our findings help shed light on a relatively neglected interval of geological time and may provide a contribution to the process of identifying a GSSP for the Norian.

Geological setting

The northwestern Sichuan Basin is a portion of the Longmen Shan foreland basin that now crops out as part of the Longmen Shan thrust belt, at the boundary between the western Sichuan Basin and Songpan–Ganzi fold belt (Fig. 1b). It was surrounded by emerged land during the Late Triassic and was connected to the Paleotethys through a large bay (Fig. 1c; Deng *et al.* 1982; Wu 1984). At the end of the Middle Triassic, collision between the North China and South China plates resulted in an extensive unconformity (Zhang *et al.*

1996; Li *et al.* 2003, 2011*a*) with the addition of NE-striking, NW-dipping extensional faults with strike-slip components (Liu *et al.* 1995). This unconformity marks the transition from the Paleozoic–Middle Triassic passive continental margin to the Longmen Shan foreland basin (Li *et al.* 2003, 2011*a*). In the early Carnian, a transgression brought the coastline from the Ganzi open marine region towards the western Sichuan Basin as far as Chengdu (Deng *et al.* 1982; Wu 1989) (Fig. 1c), and a carbonate ramp, dipping west and surrounded by locally uplifted areas, formed in the middle to western Sichuan Basin (Wu 2009; Li *et al.* 2011*b*, 2014). The Triassic stratigraphy in this region includes thick marine carbonates (*c.* 350 m in thickness) from the Ladinian (Middle Triassic) to Carnian (Late Triassic), and Carnian to Norian siliciclastic rocks (Wu 1989; Li *et al.* 2003; Mei & Liu 2017; Shi *et al.* 2017; Jin *et al.* 2018).

Three sections have been studied in this area. The Qingyan Gou section (HWQ) (31°27'46.85"N, 104°09'35.40"E), which is 9 km, and the Guanyin Ya section (HWG) (31°28'18.4"N, 104° 08'50.4"E), which is around 1.5 km, are situated in the Hanwang region. The third section is Jushui (JS) (31°30'44.6"N, 104° 13'54.5"E) near the town of Jushui (Fig. 1c). All of these sections were previously studied for their lithostratigraphy and microfacies (Wu 2009; Jin *et al.* 2015, 2018; Shi *et al.* 2017), biostratigraphy (Wu 1989; Wang 1992; Shi *et al.* 2017; Jin *et al.* 2018) and palaeomagnetic stratigraphy (Zhang *et al.* 2015).

The Middle Triassic in the northwestern Sichuan Basin

The uppermost Middle Triassic stratigraphic unit in the NW of the Sichuan Basin is the Tianjingshan Formation (T$_{2j}$), which is mainly composed of stromatolitic–bioclastic limestones or dolostones. The presence of limestone coexisting with dolostone is considered a lithological marker to identify T$_{2j}$. Such a lithology is markedly different from the overlying Carnian rocks, which comprise oolitic–bioclastic limestones and overlying hexactinellid sponge-bearing limestones (Wu 1989; Wendt 2001). The depositional environment of T$_{2j}$ is interpreted as an evaporitic tidal flat (Wu 1989). Wu (1989) assigned T$_{2j}$ to the Ladinian (Middle Triassic) on the basis of bivalve and brachiopod faunas. However, He (1980) reported a Carnian foraminiferal association including *Diplotremina* sp., *Turritellella* sp., *Ophthalmidium exiguum*, *Eoguttulina* sp., *Palaeomiliolina tibetica*, *Involutina* sp., *P. tenuis*, *Aulotortus* sp., *Gaudryina* sp. and Nodosariidae (*Astacolus*, *Frondicularia*, *Lenticulina*, *Nodosaria*, etc.), in the upper portion of the unit. Furthermore, ammonoids (*Thisbites* sp.) and conodonts (*Neogondolella polygnathiformis*, *N. navicula*) from the study by Wang & Dai (1981) suggest an upper Carnian age, but those fossils were not illustrated and are more typical of the overlying Ma'antang Formation (T$_{3m}$) (e.g. Wang 1992; Shi *et al.* 2017). The top of the Tianjingshan Formation is marked by an extensive, basin-scale unconformity surface within the stromatolitic limestone (Li *et al.* 2003, 2011*a*). This unconformity is clearly seen in the lowest part of the HWG section (Fig. 2).

The Upper Triassic (Carnian and Norian) in the northwestern Sichuan Basin

The Tianjingshan Formation is overlain by the Ma'antang Formation (T$_{3m}$) of Carnian age (Wu 1989; Wang 1992). The Carnian succession consists of two parts (Li *et al.* 2003, 2014). In our studied sections, the lower part is *c.* 55 m thick, and it begins with oolitic–bioclastic limestones, followed by hexactinellid sponge-bearing limestones and sponge mounds in an upward-deepening succession (Jin *et al.* 2018). Its sedimentary environment comprises a carbonate ramp (Wu 2009; Jin *et al.* 2018). The upper part is >65 m thick and is composed of dark grey shales, mudstones and siltstones (Li *et al.* 2003). Its sedimentary environment is

controversial, having been interpreted as a gulf (Wu 1989), foredeep (Li *et al.* 2014) and lagoon (Shi *et al.* 2015). In this paper we use the facies model of Li *et al.* (2014) (Fig. 2). The abrupt lithological change from limestone to shale has been associated with the CPE (Shi *et al.* 2009, 2017; Wang *et al.* 2015). On the basis of conodont biostratigraphy, Jin *et al.* (2018) suggested instead that the whole T$_{3m}$ succession in the Hanwang area is Tuvalian (late Carnian) and the carbonate crisis in this region is thus unrelated to the CPE.

The T$_{3m}$ is subdivided into four units (Shi *et al.* 2017; Jin *et al.* 2018): Unit 1 comprises oolitic limestones; Unit 2 consists of bioclastic limestones; Unit 3 is mainly composed of microbial sponge mounds; Unit 4 consists of siltstones and shales (Fig. 2). The oolitic–bioclastic units (Unit 1 and Unit 2 in Fig. 2) in the Hanwang area have been assigned to the lower Carnian (Julian), based on ammonoids *Protrachyceras* cf. *victoria*, *Clionites* sp., *Sandlingites* sp. and *Californites*? sp. (Wu 1989) and conodont *Paragondolella* (=*Quadralella*) *polygnathiformis*. Recently, Jin *et al.* (2018) suggested that the conodont associations from the HWQ section consisted of *Carnepigondolella angulata*, *Hayashiella tuvalica*, *Paragondolella noah*, *Carnepigondoella orchardi*, *Epigondolella miettoi* and *Carnepigondoella* cf. *orchardi*. These are typical late Tuvalian (late Carnian) conodonts (Mazza *et al.* 2012; Rigo *et al.* 2012, 2018). Wang (1992) reported ammonoids above the sponge mounds (lower part of Unit 4) in the Hanwang area that were determined as *Thisbites borellii*, *T. haushoferi*, *T.* cf. *borni*, *T. agricolae*, *Anatomites herici*, *Discotropites plinii*, *Timortropites dubvosus*, *Anatibetites* sp., *Thisbites* sp. and *Juvavites* sp. In particular, the ammonoid *Discotropites plinii* defines the uppermost late Carnian (Tuvalian 3) biochronozone (Krystyn 1982).

The overlying thick succession (*c.* 500 m thick in the studied area) of coarser terrigenous rocks is the Xiaotangzi Formation (Fig. 2). Li *et al.* (2003) attributed this stratigraphic interval to the Xujiahe Formation (T$_{3x}$). In the present study, we use the term 'Xujiahe Formation' only for the upper, coarse-grained siliciclastic unit within the Late Triassic of the Sichuan Basin.

The Xiaotangzi Formation (T$_{3xt}$) is dated as Norian based on ammonoids (Wu 1989) and bivalves (Gou 1998). The uppermost T$_{3xt}$ is characterized by quartz-lithic arenites with calcite cement. Its sedimentary environment is thought to vary from shelf to littoral (Mei & Liu 2017). To date, the biostratigraphy has been poorly determined across the CNB interval. Some researchers have proposed the occurrence of coarse quartzose sandstone as a marker of the CNB (Deng *et al* 1982; Li *et al.* 2003; Shi *et al.* 2015). Zhang *et al.* (2013) suggested that a local unconformity exists between the T$_{3m}$ and T$_{3xt}$, and this unconformity could correspond to the CNB (Fig. 2). In some localities, such as the Emei area (Fig. 1c), the upper part of T$_{3m}$ consists of shales and siltstones, and this unit is locally named the Kuahongdong Formation (Wu 1989).

Li & Wang (2016) investigated the palynological assemblages in the western Sichuan Basin, including the area of this study. Those researchers recognized three assemblages: a *Dictyophyllidites–Corollisporites–Micrhystridium* (DCM) assemblage mainly occurring in the Ma'antang Formation, a *Dictyophyllidites–Kyrtomisporis–Canalizonospora* (DKC) assemblage mainly in the Kuahongdong Formation (upper Ma'antang Formation) and a *Dictyophyllidites–Lunzisporites–Chasmatosporites* (DLC) assemblage that is the main association in the Xiaotangzi and Xujiahe formations.

In summary, only sparse biostratigraphic data from the Ma'antang, Xiaotangzi and Xujiahe formations are available, which suggests that the Carnian and Norian are both present in the studied area.

Magnetostratigraphy in the HWQ section, Hanwang area

The HWQ section has been also investigated for its magnetic polarity pattern (Zhang *et al.* 2015) and tentative correlations with
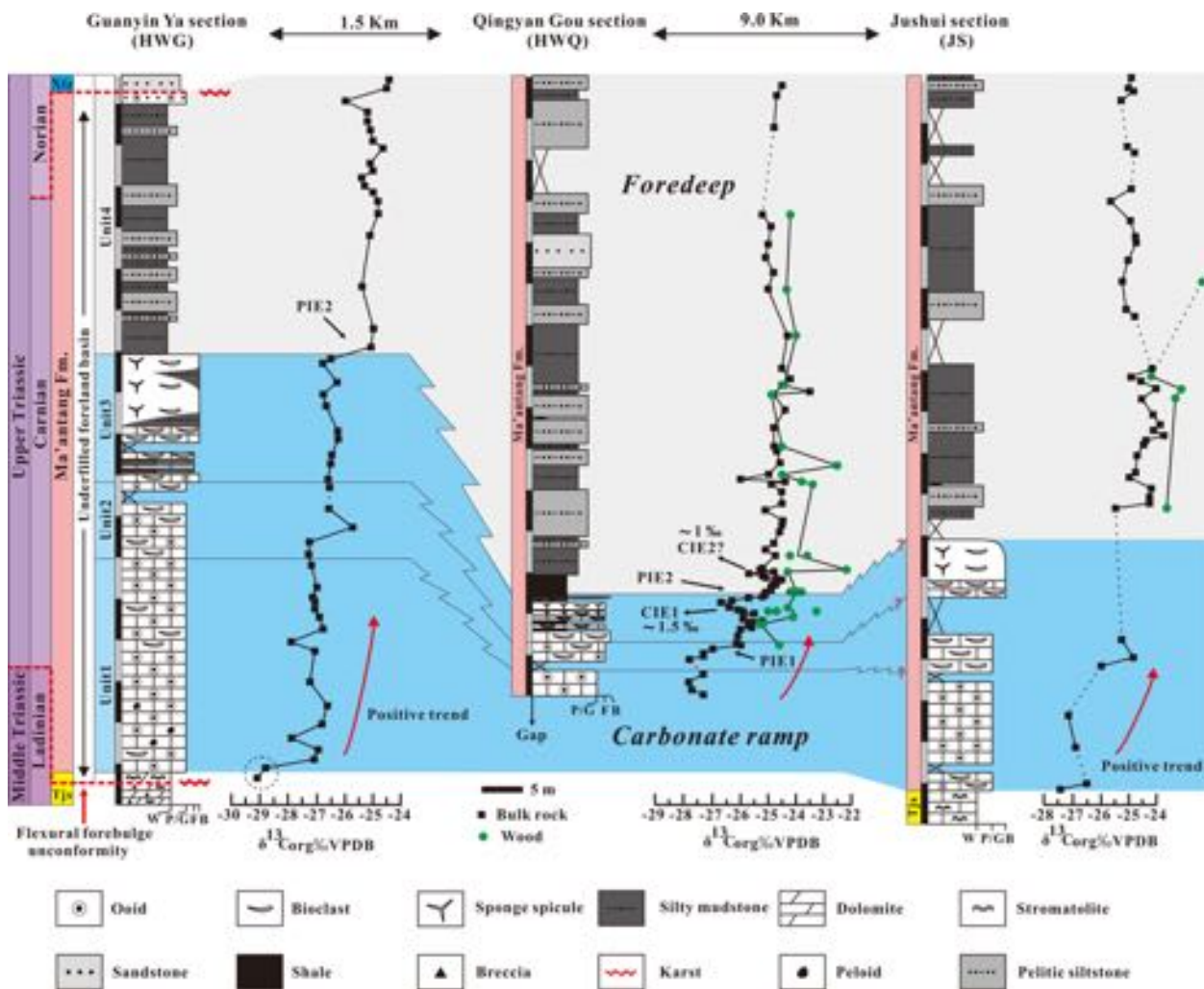
Fig. 2. Facies correlations (jagged line) and $\delta^{13}C_{org}$ values of bulk-rock and wood from the HWG, HWQ and JS sections. Lithological units (Unit 1–4) were introduced by Shi *et al.* (2017) and Jin *et al.* (2018). The term 'flexural forebulge unconformity' follows Li *et al.* (2003), and facies model follows Li *et al.* (2014). W, wackestone; P/G, packstone–grainstone; F, floatstone; B, boundstone; CIE, carbon isotopic excursion; PIE, positive isotopic excursion; Tjs, Tianjingshan Formation; Xtz, Xiaotangzi Formation.

the Triassic Astrochronostratigraphic Polarity Time Scale (APTS) have been proposed (Zhang *et al.* 2015; Shi *et al.* 2017). The latest proposed correlation implies that the HWQ section spans the lower to upper Carnian with a short interruption owing to a hiatus, which was ascribed to a karstic surface, in the middle of our Unit 3 (corresponding to the middle of Unit 2 in the HWQ section of Shi *et al.* 2017). The above-cited researchers supposed that the late Julian is missing, on the basis of their magnetostratigraphy. However, no petrographic and field evidence of karst was found by Jin *et al.* (2018).

Methods

Ammonoids, bivalves and conodonts

Ammonoids were collected from the HWQ and JS sections (A–H horizons in Fig. 3). Tens of bivalves were collected from the HWQ and JS sections in 2012 (Ba and Bb horizons in Fig. 3), but only a few of them were illustrated by Shi *et al.* (2017). Collected specimens were cleaned and photographed at the Department of Geosciences, Padova University. Two rock samples, 3–5 kg each, were also collected from the lowest part of the JS section for conodont biostratigraphy (positions a and b in Fig. 3). The conodont samples were etched with formic acid, and the residues were dried at the Institute of Sedimentary Geology, Chengdu University of Technology. Conodonts were concentrated by heavy liquid

treatment, separated manually by binocular microscope and photographed with a CamScan MX 2500 SEM in the Department of Geosciences, Padova University.

Palynology

Three palynological samples (PA–PC) were collected in the HWG and one (PD) in the HWQ section (Fig. 3). The samples were ground and *c.* 10 g of powder was treated with 10% HCl to remove the sulphates and carbonates, followed by 47% HF at 55°C, to remove silicate minerals. Residues were washed with deionized water until neutrality was reached, and were then sieved at 15 μm. The residue was stored in glycerin jelly. All the slides were studied and photographed in the Geoscience Department of Padova University.

Organic carbon isotopes

Seventy-six bulk-rock samples and 30 wood fragments from the HWQ section, 51 bulk-rock samples from the HWG section, and 40 bulk-rock samples and five wood fragments from the JS section were collected to be analysed for their $\delta^{13}C$. (From now on, the notation $\delta^{13}C_{org}$ will be used for the stable isotopic composition of organic carbon.) Bulk-rock samples were first cleaned with deionized water, then oven-dried at 50°C for one night and pulverized using an agate mortar. Subsequently, the carbonates
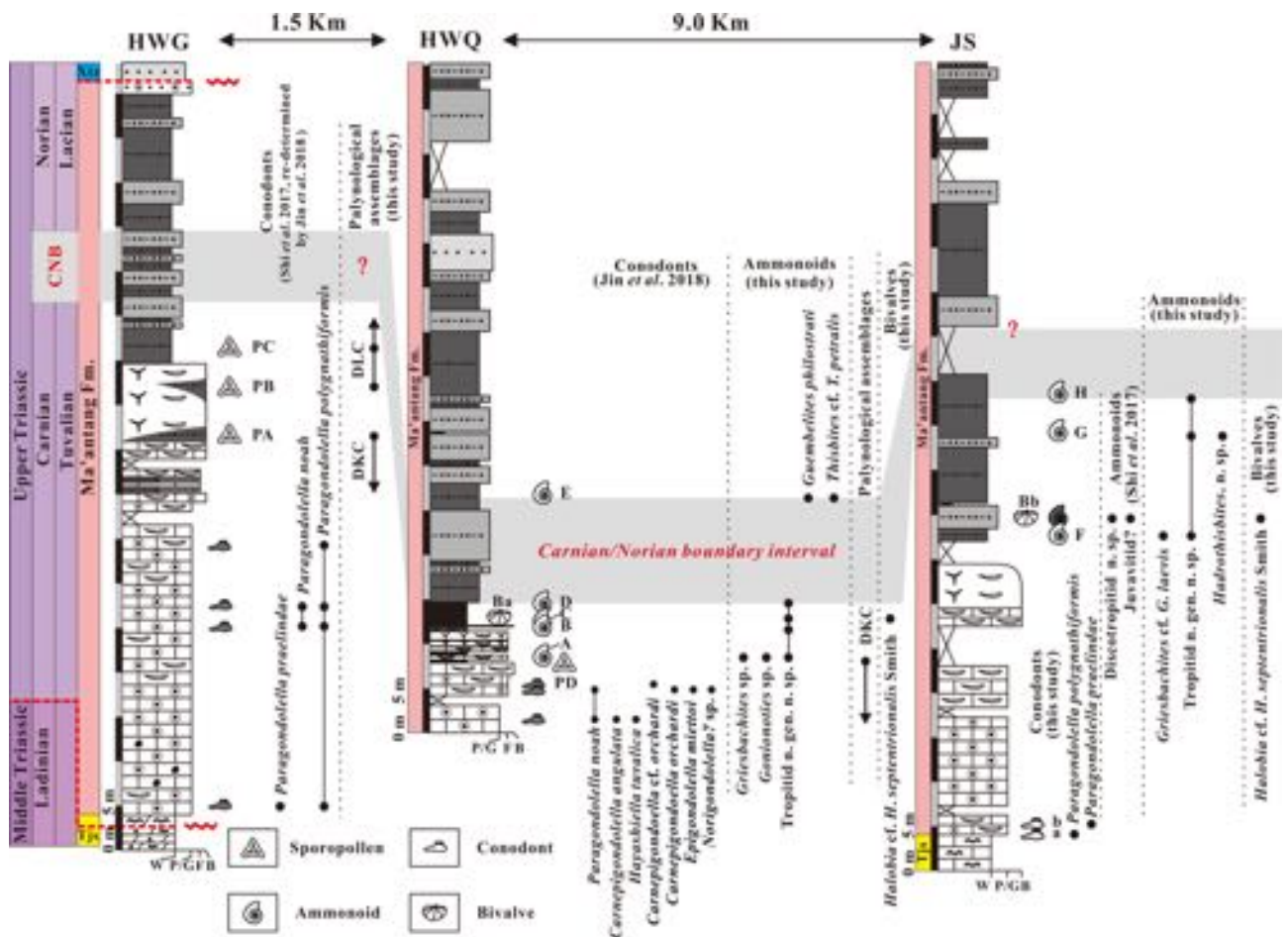
Fig. 3. Biostratigraphic data (ammonoids, conodonts, bivalves and palynological assemblage zones) and tentative correlation. The CNB (in grey) at HWQ is the uncertain interval between the last Carnian ammonoid associations with tropitids and the first Norian ammonoid associations. Palynological assemblage zones: DKC, *Dictyophyllidites–Kyrtomisporis–Canalizonospora* assemblage; DLC, *Dictyophyllidites–Lunzisporites–Chasmatosporites* assemblage (Li & Wang 2016). Letters besides fossil occurrences (A–H for ammonoids; a, b for conodonts; Ba, Bb for bivalves; PA–PD for palynomorphs) are the names of fossiliferous horizons and palynological samples used in the text.

were removed by putting *c.* 2 g of powder into a polypropylene Falcon tube with 50 ml of 10% HCl. Desulphurization was carried out for sulphurous samples with 37% HCl poured into the same tubes at 55°C for 4 h. The process was repeated until the solution lost its yellow colour. The residuals were rinsed with deionized water and centrifuged until neutrality was reached, then oven-dried again. Approximately 1–5 mg of sample were weighed into tin capsules. Wood samples were separated from bulk-rock, etched with 10% HCl and oven-dried. Approximately 0.04 mg of treated wood was weighted into tin capsules. All samples were run in duplicate. The $\delta^{13}C_{org}$ analyses were performed in the Department of Geosciences, University of Padova, with a Thermo Flash 2000 Elemental Analyzer linked to a Thermo-Delta V Advantage isotopic ratio mass spectrometer. Results were calibrated to the international VPDB scale, by analysing contemporaneously two international standards CH-7 (−32.151‰) and CH-6 (−10.449‰). A quality control standard was also run along with the samples (ZER sucrose from a C3 plant). The accuracy was *c.* ±0.15‰ (1σ) during the period of the analyses.

Results

Biostratigraphy

Conodonts

Three conodonts were found in two samples from the JS section (Fig. 3). One conodont species, *Paragondolella polygnathiformis*

(Fig. 4a), occurs in a sample within the top of stromatolite bed. In sample b (Fig. 3), above the stromatolite, the conodont species *Paragondolella praelindae* (Fig. 4b) was found. All conodonts show a Colour Alteration Index (CAI) of 1.

Ammonoids

Ammonoids were collected from five horizons in units 3 and 4 of the HWQ section (A–E in Fig. 3) and three horizons (F–H) of the JS section (Fig. 3). Ammonoids occur along with a diverse fauna that includes brachiopods and molluscs, including thin-shelled halobiid bivalves. Ammonoids are sometimes preserved with their original aragonitic shell, sometimes shells are replaced by calcite and suture lines are seldom visible. The distribution of all ammonoids from the HWQ and JS sections is displayed in Table 1.

Most specimens belong to a small (<2 cm) taxon of ammonoids with a keeled rounded venter and ventrolateral shoulders, with a moderately open umbilicus of <30% of the shell diameter. These ammonoids are densely ribbed (Fig. 5B1, B2, G1 and H), showing 10–12 ribs per quadrant on the ventrolateral margin that terminate before the keel on faint bullae or swellings. This taxon corresponds to 'Discotropitid (n. gen. n. sp. 1)' of Shi *et al.* (2017) and is here identified as 'Tropitid n. gen. n. sp.' Some specimens expose the suture line (Fig. 5G1), which is ammonitic, confirming the attribution of this taxon to the tropitid family. Tropitid n. gen. n. sp. is by far the most abundant ammonoid in horizons A, B, C and D of the HWQ section, and F, G and H of the JS section.
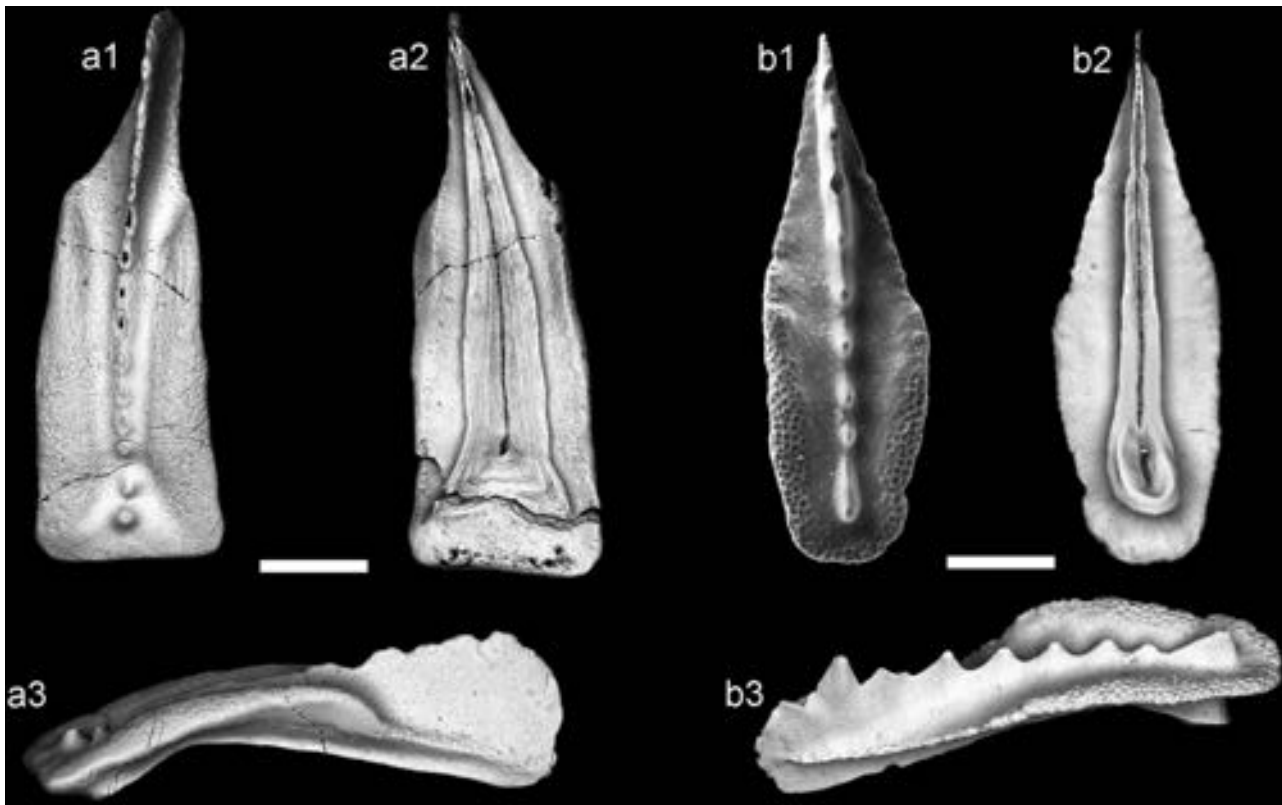
Fig. 4. Scanning electron microscope photomicrographs of conodonts from the Jushui section. (**a**) *Paragondolella polygnathiformis*; (**b**) *Paragondolella praelindae.* For each specimen: (1) upper view, (2) lower view, (3) lateral view. '**a**' and '**b**' refer to the sampling horizons (see Fig. 3). CAI=1 All scale bars represent 200 μm.

Involuted, smooth ammonoids were also collected that are attributed to the family Juvavitidae. A specimen from horizon A at HWQ (Fig. 5A1) is *c.* 3 cm in diameter and is preserved as a compressed replaced shell. The venter and suture lines are not visible; however, weak ribs are visible in the outer part of the flank that disappear in the umbilical part. This specimen was determined as *Gonionotites* sp. Several specimens were collected of an ammonoid taxon with smooth, involute shell and an elliptical whorl section that we tentatively attribute to the genus *Griesbachites* (e.g. Fig. 5A2, F1 and F2). These have a rounded venter without ornamentation, and flanks with few coarse and simple ribs or plicae that near the venter are adorally projected and terminate without bullae or knots. One specimen from the JS section exhibits the suture line partially (Fig. 5F1) at a diameter of *c.* 2 cm. This suture line has at least three lobes and three saddles, all deeply denticulated and squared, the first lobe being deeper than all others. This suture line and the weak ornamentation compare well with that of *Griesbachites laevis* illustrated by Tozer (1994), in which the ventrolateral bullae that are typical in large specimens of *Griesbachites* are instead missing or minimally developed. The 'Juvavitid, n. gen.' of Shi *et al.* (2017) most probably belongs to this taxon.

A fragment of a strongly ribbed, involuted ammonoid, preserved as an external mould, was collected from horizon E of the HWQ section (Fig. 5E1). This specimen compares well with the inner whorls of *Guembelites philostrati* illustrated by Krystyn (1982, plate 13, fig. 6) from the Jomsom section in the Nepalese Himalaya. From the same horizon, we also collected a fragmented specimen of *Thisbites* (Fig. 5E2). This ammonoid shows a dense ribbing, with 17 ribs being counted per quadrant at a diameter of *c.* 1 cm. Ribs are falcoid, mostly simple, a few are bifurcated close to the umbilical margin, and the ribs terminate on strong tubercles alongside a keeled venter. This specimen can be clearly distinguished from Discotropitid n. gen. n. sp. 1 because of the denser ribs, which terminate on strong tubercles instead of the weak bullate swellings of Tropitid n. gen. n. sp. Because of the dense ribbing and strong tubercles, this *Thisbites* has been determined as *Thisbites* cf. *petralis* (see Tozer 1994, plate 108, figs 3 and 4).

Finally, a nearly complete specimen of an ammonoid with distinctive ornamentation comes from horizon G of the JS section (Fig. 5G2). This specimen, *c.* 1.5 cm in diameter, has a narrow, keeled venter bordered by bullated tubercles on the ventrolateral shoulders. The umbilicus is well open and exposes ribbed inner whorls. The last whorl, probably a habitation chamber, is not ribbed, and shows only very weak tubercles elongated radially that mimic faint ribs. Of the suture line, only part of an entire saddle is visible. We attribute this ammonoid to a species of *Hadrothisbites* different from *H. taylori* of Tozer (1994).

Table 1. *Late Triassic ammonoids in northwestern Sichuan Basin, China*

| Ammonoid species	Horizon	Occurrence	Section
Tropitid n. gen. n. sp.	A	XX	HWQ
Tropitid n. gen. n. sp.	B	XX	HWQ
Tropitid n. gen. n. sp.	C	X	HWQ
Tropitid n. gen. n. sp.	D	X	HWQ
Tropitid n. gen. n. sp.	F	X	JS
Tropitid n. gen. n. sp.	G	XX	JS
Tropitid n. gen. n. sp.	H	XX	JS
Gonionotites sp.	A	X	HWQ
Griesbachites sp.	A	X	HWQ
Griesbachites cf. *laevis*	F	X	JS
Guembelites philostrati	E	X	HWQ
Thisbites cf. *petralis*	E	X	HWQ
Hadrothisbites n. sp.	G	X	JS
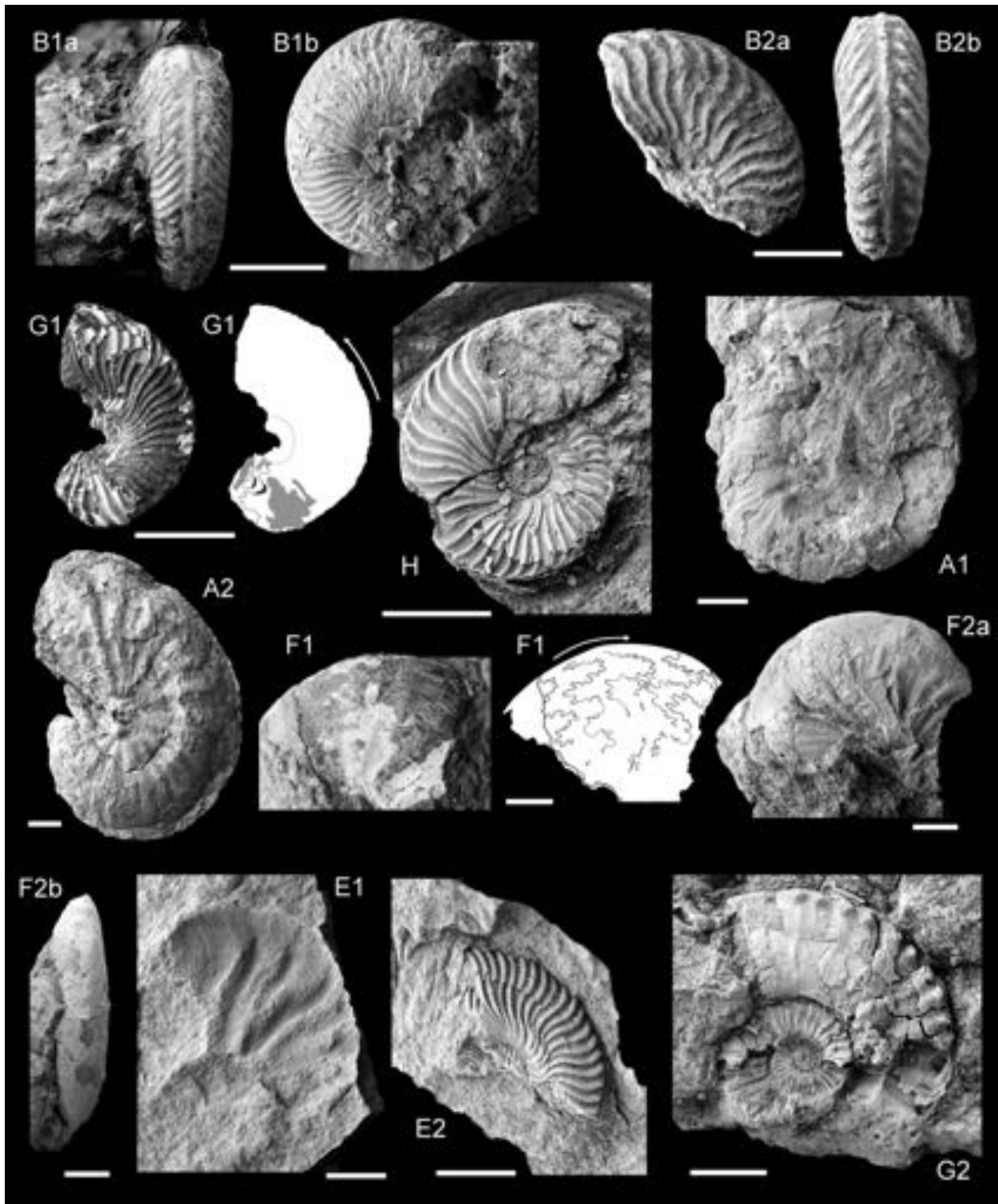
Fig. 5. Photographs of ammonoids from the HWQ and JS sections. Letters refer to sampling horizons (see Fig. 3). (B1, B2, G1, H) Tropitid n. gen. n. sp.; (A1) *Gonionotites* sp.; (A2, F2) *Griesbachites* sp.; (F1) *Griesbachites* cf. *laevis*; (E1) *Guembelites philostrati*; (E2) *Thisbites* cf. *petralis*; (G2) *Hadrothisbites* n. sp. For (B1), (B2) and (F2): (a) upper view, (b) lateral view. All scale bars represent 5 mm.

The association of tropitids, *Hadrothisbites* n. sp., *Gonionotites* sp. and *Griesbachites* sp. at HWQ and JS indicates a late Tuvalian (late Carnian) age. In particular, tropitids are known so far only from the upper Carnian. It should be noted, however, that the tropitids illustrated in the present paper are a new taxon, whose distribution is thus unknown. The ammonoids from horizon E of the HWQ section suggest instead an early Norian age: *Guembelites philostrati* is so far known only from the Norian, whereas the species of genus *Thisbites* occur in a short stratigraphic interval across the Carnian–Norian

boundary; *T. petralis*, however, is known only from the lower Norian (Tozer 1994).

Bivalves

Halobiid bivalves occur at several levels (Ba and Bb) within both the HWQ and JS sections (Fig. 3). Most of the specimens are preserved as partial skeletons of recrystallized calcite, which expose the outer surface of a middle skeletal layer. Although this surface
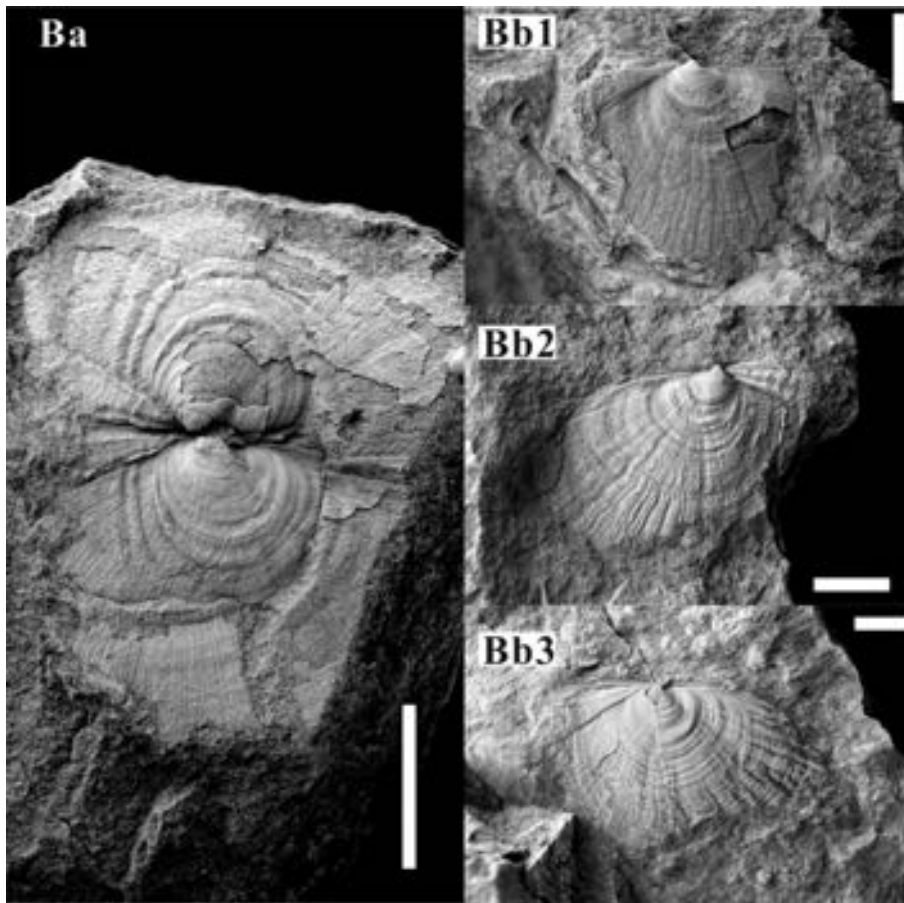
Fig. 6. Photographs of *Halobia* cf. *septentrionalis* Smith from the HWQ (Ba) and JS (Bb1–3) sections. Ba, articulated valve pair; Bb1, left valve; Bb2, right valve; Bb3, left valve. All scale bars represent 1 cm.

(between the shell layers) does preserve some of the original ornament of the individuals (e.g. commarginal growth banding and at least the general course and direction of the radial ornament), details of the external expression of radial ribs from the outer skeletal layer are obscured, precluding definitive species-level identification.

Based on shell outlines, commarginal growth banding, the angular breadth of the anterior tube and generalized course of the ribbing of the specimens, it appears highly probable that they belong to a single species, here referred to as *Halobia* cf. *septentrionalis* Smith (Fig. 6), and may therefore may serve as a robust correlation datum between the two sections. The HWQ and JS specimens are similar to those that have been attributed to both *Halobia qaboensis* Zhang and *Halobia septentrionalis* Smith. There is a strong possibility of these two taxa being synonymous. Chen & Ba (1986, plate 2, figs 6, 8, 11 and 14) illustrated *Halobia septentrionalis* Smith 1927 from the middle to late Carnian of Zedang (south Xizang). This species is known from several localities throughout North America, and is perhaps best represented in southeastern Alaska and western Canada in the upper Carnian (*K. macrolobatus* ammonoid zone) as discussed by McRoberts (2010, 2011). This morphotype is also similar to *Halobia qaboensis* Zhang (of Zhang *et al.* 1985, plate 33, figs 1–9) known from the Bolila Formation, near Kangba and Chengdu. However, the preservation of Zhang's illustrated specimens is rather poor, making direct comparisons with *H. septentrionalis* not possible. Additionally, the HWQ and JS halobias may be compared with those Ma *et al.* 1976 (plate 33, fig. 6) referred to as *Halobia rugosa* Gümbel from the Yunnanyi Formation, Xiangyun County, Yunnan. More recent evaluations of *Halobia rugosa* (see McRoberts 2011; Levera 2012) suggest that '*H. rugosa*' from the late Carnian are distinctively different from true *Halobia rugosa*, which is earliest Carnian (=*Trachyceras* ammonoid zone) from

the western Tethys. Therefore, it is possible that the Yunnanyi '*H. rugosa*' are also conspecific with those described as *Halobia* cf. *septentrionalis* in this paper (Fig. 6).

The morphological affinities of the HWQ and JS *Halobia* cf. *septentrionalis* suggest a Tuvalian age and are most probably a mid- to upper Tuvalian equivalent to the *Anatropites* (= *K. macrolobatus*) or slightly older *T. subbulatus* (= *T. welleri*) ammonoid zones (*sensu* Silberling & Tozer 1968; Kozur 2003; McRoberts 2010).

Spores and pollen

The sporomorphs were collected from PA–PC and PD positions from the HWG and HWQ sections (Fig. 3), respectively. The preservation of the palynological material is unfortunately not good, because of degradation on the exine. Representative sporomorphs are shown in Figure 7, and the distribution of all sporomorphs is shown in Table 2.

The spores from the HWG section are composed of levigated and ornamented Azonotriletes *Deitoidospora* sp., *Concavisporites* spp, *Dictyophyllidites* sp., *Dictyophyllidites harrisii*, *Todisporites* sp., *Punctatisporites* spp., *Converrucosisporites* spp., *Verrucosisporites* sp., *Pustulatisporites* sp. and *Leiotriletes* sp.; cingulati spores *Annulispora* sp., *Stereisporites* sp. and *Asseretospora* sp.; zonate spore *Kraeuselisporites* sp.; cavatomonoletes *Aratrisporites* spp.; and a cingulicavate form *Densosporites* sp. Pollen grains are rare, including alete forms *Psophosphaera* spp. and *Araucariacites* sp.; and monocolpate forms *Riccisporites* sp., *Cyadopites* sp. and *Chasmatosporites* spp. Bisaccates *Piceites* sp. and *Pinuspollenites enodatus*, and green algae spores *Tasmanites* sp. are present.

The spores from the HWQ section consist of Azonotriletes *Concavisporites* sp., *Converrucosisporites* sp. and *Anapiculatisporites* sp.; zonate spore *Kraeuselisporites* sp.; and cavatomonoletes *Aratrisporites* sp. The pollen grains contain the monocolpate
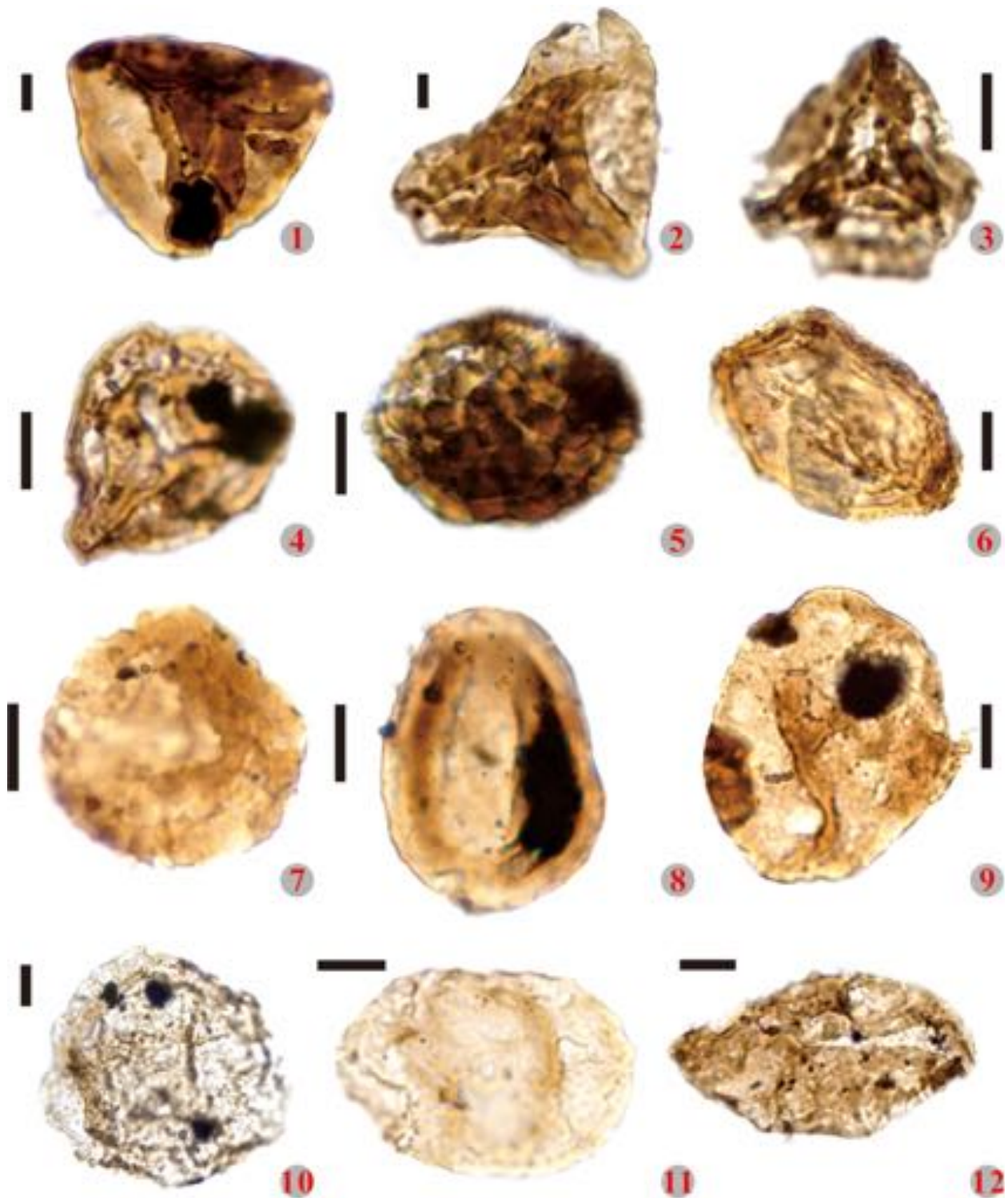
Fig. 7. Representative palynomorphs from the HWG and HWQ sections. (1) *Concavisporites* sp., sample PD, HWQ; (2) *Pustulatisporites* sp., sample PC, HWG; (3) *Concavisporites* sp., sample PC, HWG; (4) *Stereisporites* sp., sample PB, HWG; (5) *Verrucosisporites* sp., sample PB, HWG; (6) *Kraeuselisporites* sp., sample PB, HWG; (7) *Converrucosisporites* sp., sample PD, HWQ; (8) *Chasmatosporites* sp., sample PD, HWQ; (9) *Psophosphaera* sp., sample PB, HWG; (10) *Araucariacites* sp., sample PA, HWG; (11) *Pinuspollenites* sp., sample PD, HWQ; (12) *Cyadopites* sp., sample PA, HWG. All scale bars represent 10 μm.

Cyadopites sp. and *Chasmatosporites* spp., bisaccates *Pinuspollenites* sp. and *Alisporites* sp.; and algae spores *Botryococcus* sp. and *Tasmanites* sp.

$δ^{13}C$ of bulk organic matter from woods and bulk-rock

The $δ^{13}C_{org}$ values at the HWG section range from −29.12 to −24.39‰, those from the HWQ section range between −27.84 and −23.47‰, and those from the JS section vary from −27.47 to −23.90‰. In the HWQ section, 30 wood fragments were collected, and their values range from −25.35 to −22.37‰. The values of five wood samples from the JS section range between −24.29 and −22.07‰. The $δ^{13}C$ data from limestone, terrigenous rocks and wood are distinct (Fig. 8).

The mean value of $δ^{13}C_{org}$ in limestones from the three sections is −26.6‰, whereas terrigenous rocks of the Ma'antang Formation

Table 2. *Late Triassic palynomorphs in the Hanwang area, northwestern Sichuan Basin*

Palynomorph	Samples	Occurrence	Section
Alisporites sp.	PD	X	HWQ
Anapiculatisporites sp.	PD	X	HWQ
Annulispora sp.	PA	X	HWG
Aratrisporites spp.	PA, PB, PD	XX	HWG, HWQ
Araucariacites sp.	PA, PB, PC	X	HWG
Asseretospora sp.	PB	X	HWG
Bisaccates	PA, PB	X	HWG
Botryococcus sp.	PD	X	HWQ
Chasmatosporites spp.	PB, PC, PD	XX	HWG, HWQ
Concavisporites sp.	PA, PB, PC, PD	X	HWG, HWQ
Converrucosisiporites spp.	PA, PD	XX	HWG, HWQ
Cyadopites spp.	PA, PB, PD	XX	HWG, HWQ
Deitoidospre sp.	PC	X	HWG
Densosporites sp.	PA	X	HWG
Dictyophyllidites harrisii	PB	X	HWG
Dictyophyllidites sp.	PC	X	HWG
Kraeuselisporites sp.	PA, PB, PD	X	HWG, HWQ
Leiotriletes sp.	PA	X	HWG
Piceites sp.	PA	X	HWG
Pinuspollenites enodatus	PB, PD	X	HWG, HWQ
Psophosphaera spp.	PA, PB	XX	HWG
Punctatisporites spp.	PA, PB, PC	XX	HWG
Pustulatisporites sp.	PC	X	HWG
Riccisporites sp.	PC	X	HWG
Stereisporites sp.	PB	X	HWG
Tasmanites sp.	PA, PD	X	HWG, HWQ
Todisporites sp.	PB	X	HWG
Verrucosisporites sp.	PC	X	HWG

have an average $\delta^{13}C_{org}$ value of −24.8‰. The wood fragments of the HWQ and JS sections are −24.0‰ on average: more positive than but largely overlapping with the $\delta^{13}C_{org}$ in terrigenous rocks (Fig. 8). All sections exhibit a weak positive trend in limestone units 1–3 (Fig. 2), and very negative values of about −29‰ occur at the stromatolite in the basal part of the HWG section above the unconformity surface (dashed circle in Fig. 2).

In the HWQ section, two positive isotopic excursions (PIE1 and PIE2) are observed. PIE1 is within the limestone unit, whereas PIE2 coincides with the lithological change from limestone to shale and siltstone. PIE2 can be observed in a comparable position also at the HWG section (Fig. 2).

Two short-lived negative carbon isotopic excursions (CIE1 and CIE2) are observed in the HWQ section. The first is within the sponge mound interval (uppermost Unit 3) and has a magnitude of *c.* 1.5‰. A second, negative shift of *c.* 1‰ is seen just above PIE2 (Fig. 2). These negative excursions do not occur in correlated sections, and are thus unlikely to be related to a regional signal. The wood samples are ^{13}C-enriched with respect to the coeval bulk OM, and their isotopic composition has large variability (Fig. 8).

Discussion

### The Carnian–Norian boundary interval in NW Sichuan Basin

Despite their poor species diversity, ammonoids suggest that a continuous record of the CNB is preserved in northwestern Sichuan. Ammonoids were found in the Ma'antang Formation of the Sichuan Basin also by Wu (1989) and Wang (1992), albeit the precise sampling position of their findings within a stratigraphic log was not given. They found a much richer fossil association, which we could not fully recover. However, the occurrence of *Thisbites* spp., which was found also during this study in the HWQ section, was documented by both researchers. Genus *Thisbites* is typical of the Carnian–Norian boundary interval (e.g. Tozer 1994).

Shi *et al.* (2017) illustrated an ammonoid association from the JS section that is similar to the one illustrated in the present paper (Fig. 3). The ammonoids illustrated by Shi *et al.* (2017) were collected on a large but isolated outcrop on the eastern valley flank. However, their stratigraphic position could be determined with good approximation by tracing beds in the field (Fig. 2). These ammonoids include both smooth-shelled juvavitids and abundant tropitids; Shi *et al.* (2017) interpreted this ammonoid association as representing the lower Tuvalian. Because of a richer ammonoid association presented herein, and an improved determination of smooth-shelled taxa, we are now confident that this ammonoid association instead indicates a late Tuvalian (late Carnian) to early Norian age. This ammonoid biochronology is consistent with our age determination of halobiid bivalves and conodonts.

The palynological associations also suggest a late Carnian–Norian age. Pollen and spores from the PA horizon in the HWG section and the PD horizon are similar to the DKC assemblage of Li & Wang (2016) from the Kuahongdong Formation dated to late Carnian–early Norian. Pollen and spores from the PB horizon show the appearance of some important taxa such as *Psophosphaera* and *Riccisporites*, which are similar to the DLC assemblage of Li & Wang (2016) from the Xiaotangzi and Xujiahe formations, which those researchers assumed to be Norian–Rhaetian. Moreover, the distinctive palynological associations described in the western Tethys during the Carnian Pluvial Episode (e.g. Roghi 2004; Roghi *et al.* 2010; Mueller *et al.* 2016) seem to be absent, further confirming that the stratigraphic succession in Hanwang is younger than the CPE.

The amended age of stromatolitic beds of the uppermost Tianjingshan Formation

The conodonts *Paragondolella polygnathiformis* (Fig. 4a) and *Paragondolella praelindae* (Fig. 4b) were found within or just above the stromatolitic beds of the JS section (Fig. 3). This interval
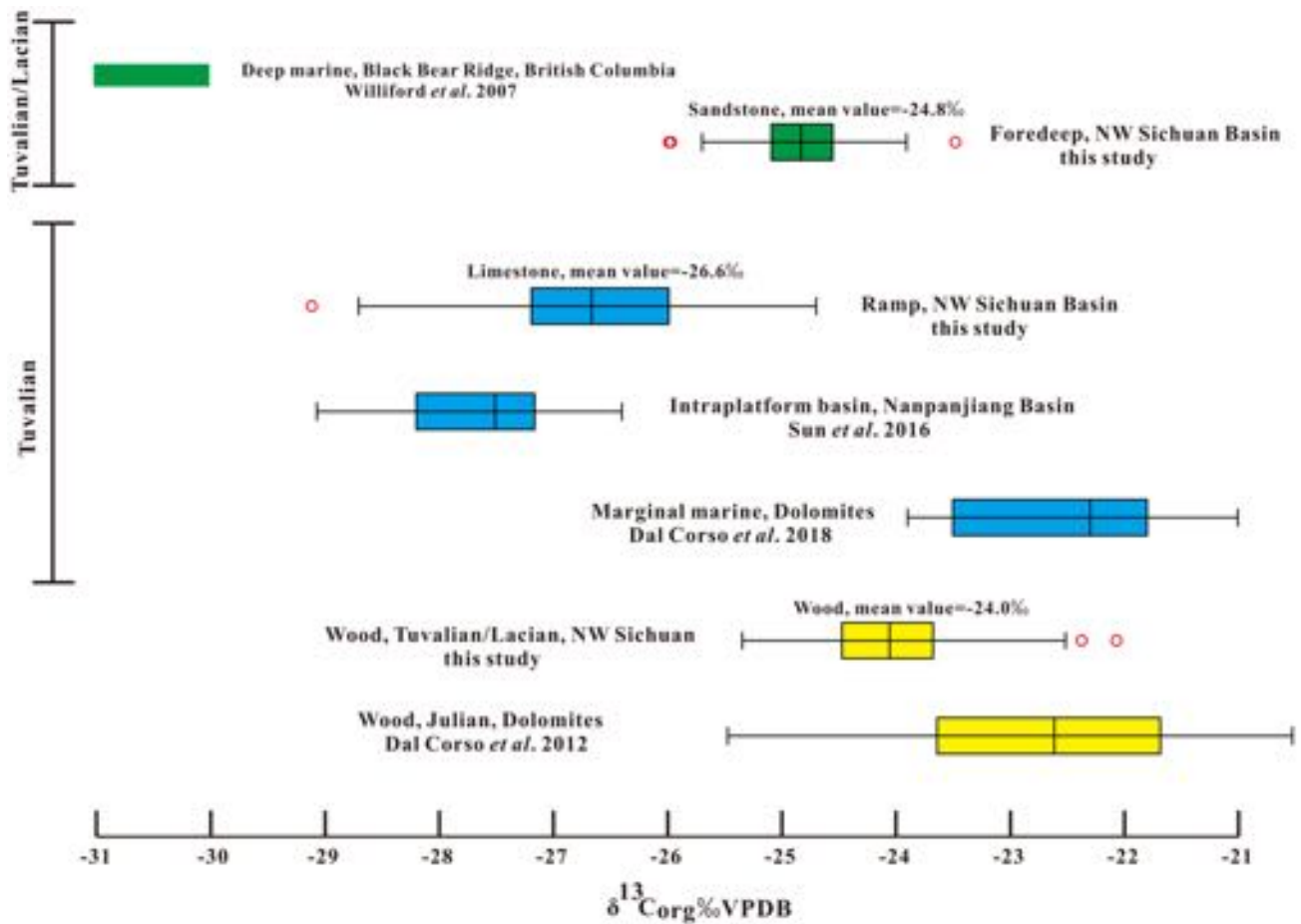
Fig. 8. Comparison of $\delta^{13}C_{org}$ values of the Carnian–Norian bulk-rock and wood from western and eastern Tethys. The boxes represent 25 and 75% quartiles, the whiskers depict 10 and 90% ranges, and the central lines in the box depict the medians. Outliers are highlighted with a red circle. For Black Bear Ridge, the full range of $\delta^{13}C_{org}$ variability is plotted instead of a box plot.

was attributed to the uppermost Tianjinshan Formation and was dated to the Middle Triassic (Wu 1989). However, *P. polygnathiformis* and *P. praelindae* are exclusive to the Julian (lower Carnian) to lower Tuvalian (upper Carnian; e.g. Mazza *et al.* 2012). *P. polygnathiformis* first appears in the Carnian GSSP section of Stuores Wiesen, very close to the Ladinian–Carnian boundary (Mietto *et al.* 2012), and is routinely used as a datum to define the Carnian. Therefore, the uppermost Tianjinshan Formation at the JS section should be assigned a Carnian age. This age determination would agree with those of, for example, He (1980) and Wang & Dai (1981).

A revised magnetostratigraphic correlation of the HWQ section

The most recent magnetic polarity timescale for the late Triassic (Kent *et al.* 2017) is mostly based on data from the Newark Basin, correlated with the biostratigraphy of western Tethys. For the Tuvalian to Lacian (i.e. late Carnian to early Norian) interval a biostratigraphically calibrated record of magnetic polarity reversals has been investigated in the Pizzo Mondello section (Sicily; Muttoni *et al.* 2001, 2004; Mazza *et al.* 2012, 2018).

The new findings of conodonts, ammonoids and halobiid bivalves at HWQ allow an amended magnetostratigraphic correlation with western Tethys and the Newark polarity timescale. However, biostratigraphic age determinations are not fully in agreement with each other at HWQ. This led us to provide two correlation proposals, each having its advantages and drawbacks.

At Pizzo Mondello, among many other taxa, the platform conodont elements *Hayashiella tuvalica*, *Carnepigondolella zoae*,

C. angulata and *Paragondolella noah* disappear at the top of the PM3r magnetozone, whereas the co-occurrence of *Epigondolella miettoi* and *Carnepigondoella orchardi* has a narrow distribution in the magnetozone PM4n, immediately below the proposed CNB defined by the FO of *Metapolygnathus parvus* (Mazza *et al.* 2018; Rigo *et al.* 2018) (Fig. 9). The conodonts *Epigondolella miettoi* and *Carnepigondoella orchardi* were found by Jin *et al.* (2018) in the HWQ section within HQ2n, below horizons with the upper Tuvalian to lower Lacian ammonoids. This implies that the whole magnetostratigraphic record at the HWQ section is younger than suggested by Zhang *et al.* (2015) and Shi *et al.* (2017). In the HWQ section, Shi *et al.* (2017) identified a karstic surface (i.e. hiatus) within HQ2r. It was suggested that the record of geomagnetic reversals at HWQ is thus discontinuous, and the late Julian is truncated (fig. 10 of Shi *et al.* 2017). However, Jin *et al.* (2018) did not find any detectable omission or erosive surface, which could correspond to a hiatus, in this interval. In light of the conodont biostratigraphy, and assuming near-constant sedimentation rates, the magnetozones in the HWQ section can be correlated to the magnetozones at Pizzo Mondello (Option A in Fig. 9). Assuming near-constant sedimentation rates means that the thickness ratios of magnetozones at HWQ are similar to those of the Newark magnetic polarity timescale.

The Option A correlation implies that the ammonoid associations of horizons A–D, which contain tropitids and *Halobia* cf. *septentrionalis*, are Norian. The CNB interval is to be placed between 6 and 9.5 m from the base of the HWQ section. However, this correlation implies low sedimentation rates through the section, generally <10 m Ma^{-1}, which seem to be unlikely in a foreland
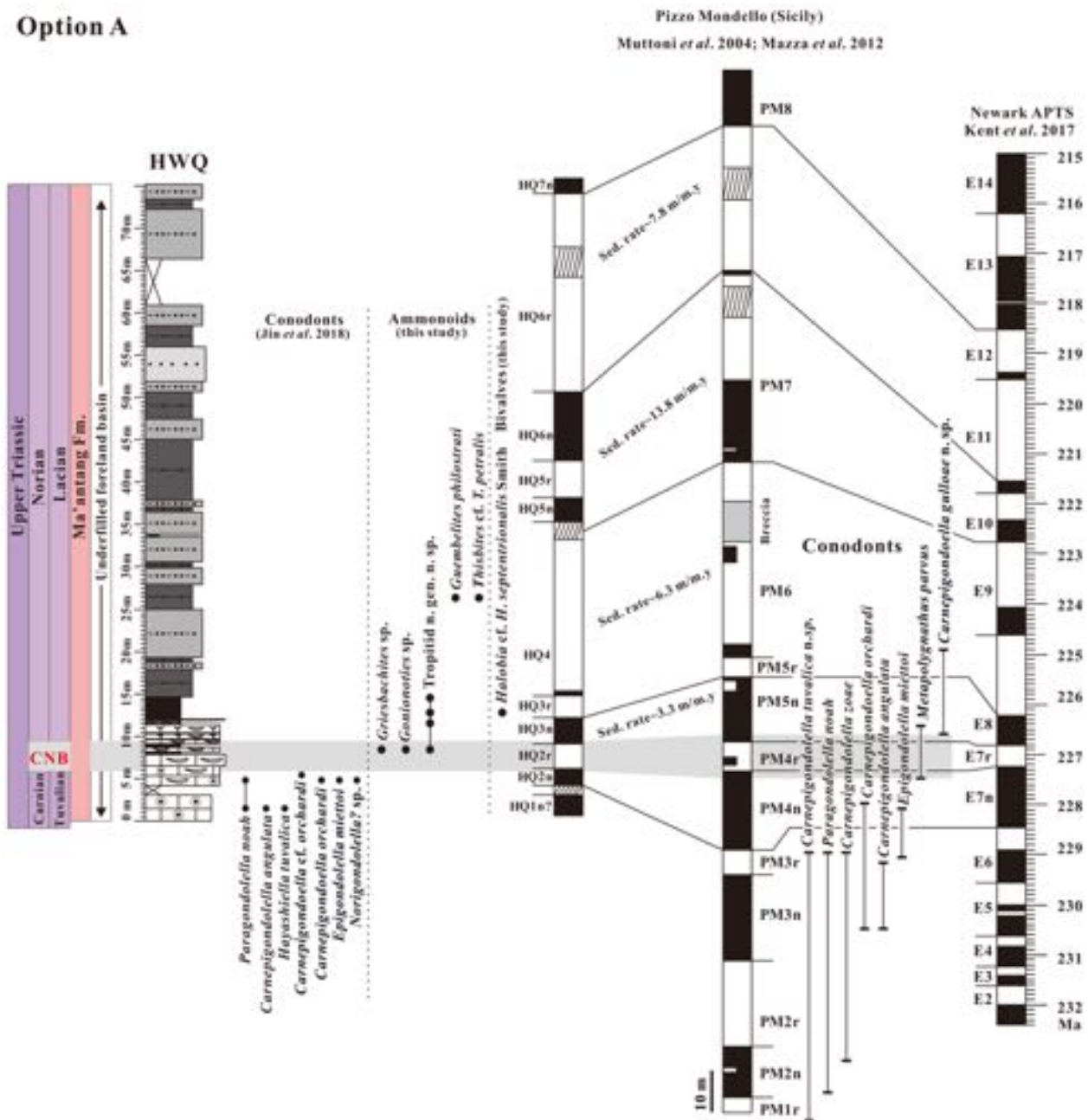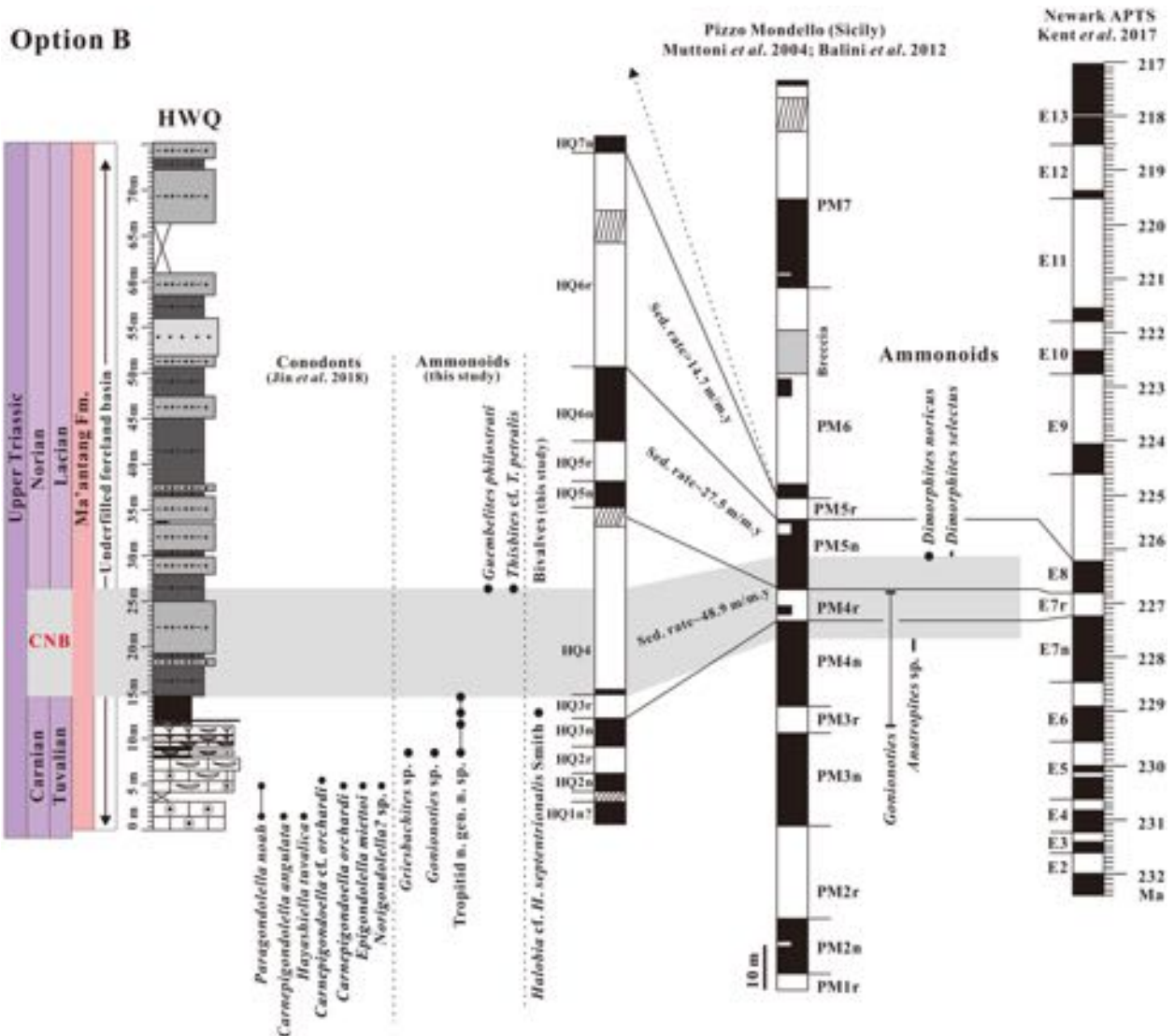
Fig. 9. Correlation of the HWQ section with the Newark Astrochronostratigraphic Polarity Time Scale (APTS) (Kent *et al.* 2017) and Pizzo Mondello, Sicily (Muttoni *et al.* 2004), based on conodont biostratigraphy and magnetostratigraphy (Zhang *et al.* 2015; Jin *et al.* 2018). The Carnian–Norian boundary (CNB) interval (in grey) is placed between 6 and 9.5 m. According to this proposal, the CNB (in grey) coincides with the boundary interval of Mazza *et al.* (2012); that is, the interval between the FO of *Metapolygnathus parvus* (conodont) and the FO of *Halobia austriaca* (bivalve) at Pizzo Mondello. This boundary interval was then correlated assuming that HQ2r above the conodonts at the HWQ section coincides with PM4r at Pizzo Mondello. With this correlation, the bivalve *Halobia* cf. *septentrionalis* would occur in the Norian at HWQ.

basin system and more typical of starved open ocean environments below the carbonate compensation depth (e.g. Enos 1991).

An alternative correlation is proposed that accounts for increasing sedimentation rates at the HWQ section that could be expected in a foreland basin (Option B in Fig. 10). The Option B correlation maintains that ammonoid horizons with tropitids and *Halobia* cf. *septentrionalis* are within the Carnian, but requires that the thickness of magnetozones at HWQ is not proportional to their duration, and these thicknesses do not correlate to those of magnetozones at Pizzo Mondello. The Carnian Ma'antang Formation is the initial sedimentation stage of the Longmen Shan foreland basin (Li *et al.* 2003, 2014). The deep marine shales and mudstones of the upper Ma'antang Formation (Fig. 2) contain deep-water fossils, suggesting that the basin was underfilled at this

stage (Li *et al.* 2003, 2014), but then, with the siltstones and sandstones of the Xiaotangzi Formation, sedimentation was keeping up with subsidence. Along with the development of the foreland basin, the sedimentation rates were increasing, and on the basis of the upper Triassic thickness of Li *et al.* (2003) and the geological timescale of Cohen *et al.* (2013), we calculated average net sedimentation rates in the studied area of *c.* 25 to *c.* 50 m Ma^{-1} in the Carnian, *c.* 162 m Ma^{-1} in the Norian and >139 m Ma^{-1} in the Rhaetian. This suggests that sedimentation rates were increasing near the CNB in the Sichuan Basin. All calculations of net sedimentation rates do not consider compaction and denudation rates, hence the original accumulation rates may have been higher. In view of ammonoids, bivalves and sedimentation rate, the reverse polarity interval PM4r at Pizzo Mondello may correlate to the

Fig. 10. Correlation of the HWQ section with the Newark APTS (Kent *et al.* 2017) and Pizzo Mondello, Sicily (Muttoni *et al.* 2004), based on ammonoid biostratigraphy (this study; Balini *et al.* 2012, for Pizzo Mondello) and magnetostratigraphy (Zhang *et al.* 2015). The Carnian–Norian boundary (CNB) interval (in grey) is placed between 14.5 and 26.5 m. In Option B, the CNB (in grey) is the uncertain interval between the last Carnian ammonoid associations with tropitids and the first Norian ammonoid associations (see also Fig. 3). This uncertain interval may not be the same between HWQ and Pizzo Mondello. Magnetozones are then correlated assuming a sedimentation rate that is increasing, on average, with time, as must be expected for a foreland basin. With this correlation, the bivalve *Halobia* cf. *septentrionalis* would occur in the Carnian at HWQ.

interval between HQ3r and the top of HQ4r at the HWQ section. According to Option B, the CNB interval at the HWQ section could be positioned between 14.5 and 26.5 m. The drawback of this correlation (Option B) is that the thickness ratios of magnetozones are not preserved, and as a result the correlation is outside of the range of biostratigraphic constraints. Further biostratigraphic investigations are needed to finally assess which of the offered correlation options is better.

The sources of OM in the Sichuan Basin

The $\delta^{13}C_{org}$ in sedimentary rocks can result from the combination of OM from diverse sources, in particular marine or freshwater–terrestrial (Fogel & Cifuentes 1993). A possible variability of OM sources in the investigated sections is demonstrated in Figure 8, where the average carbon isotopic compositions of different components from the Sichuan Basin are compared with those of coeval localities worldwide, where the provenance of OM could be suggested on the basis of the sedimentary environments. The $\delta^{13}C_{org}$ of sandstone across the CNB interval is more positive than

samples from coeval deep marine settings of Black Bear Ridge, but overlaps with that of wood samples from both the Sichuan Basin and the Southern Alps. In contrast, the average $\delta^{13}C_{org}$ of limestones in the Sichuan Basin, which bear little terrigenous material and no wood, is closer to the carbon isotopic composition of the open marine Black Bear Ridge section. These different $\delta^{13}C_{org}$ values could be easily explained if we assume that OM in limestones is mostly marine in origin, whereas the wood-bearing sandstones contain mostly terrestrial organic matter.

Recent marine OM, which is mainly derived from phytoplankton and benthic and macroscopic algae (Fry *et al.* 1977), has a $\delta^{13}C_{org}$ less negative than −23.0‰ (Fry *et al.* 1977; Anawar *et al.* 2010). However, the terrestrial OM is more $\delta^{13}C$-enriched than marine OM during the Triassic (Hayes *et al.* 1999; Nordt *et al.* 2016). OM remineralization, metabolic fractionation and diagenesis could alter the isotopic composition of OM (e.g. McArthur *et al.* 1992; Goñi *et al.* 1997; Anawar *et al.* 2010), but the impact of diagenetic factors should not be important in our case, because we consider only relative changes within bulk-rock and wood, which were affected by similar diagenetic influences in each study area.
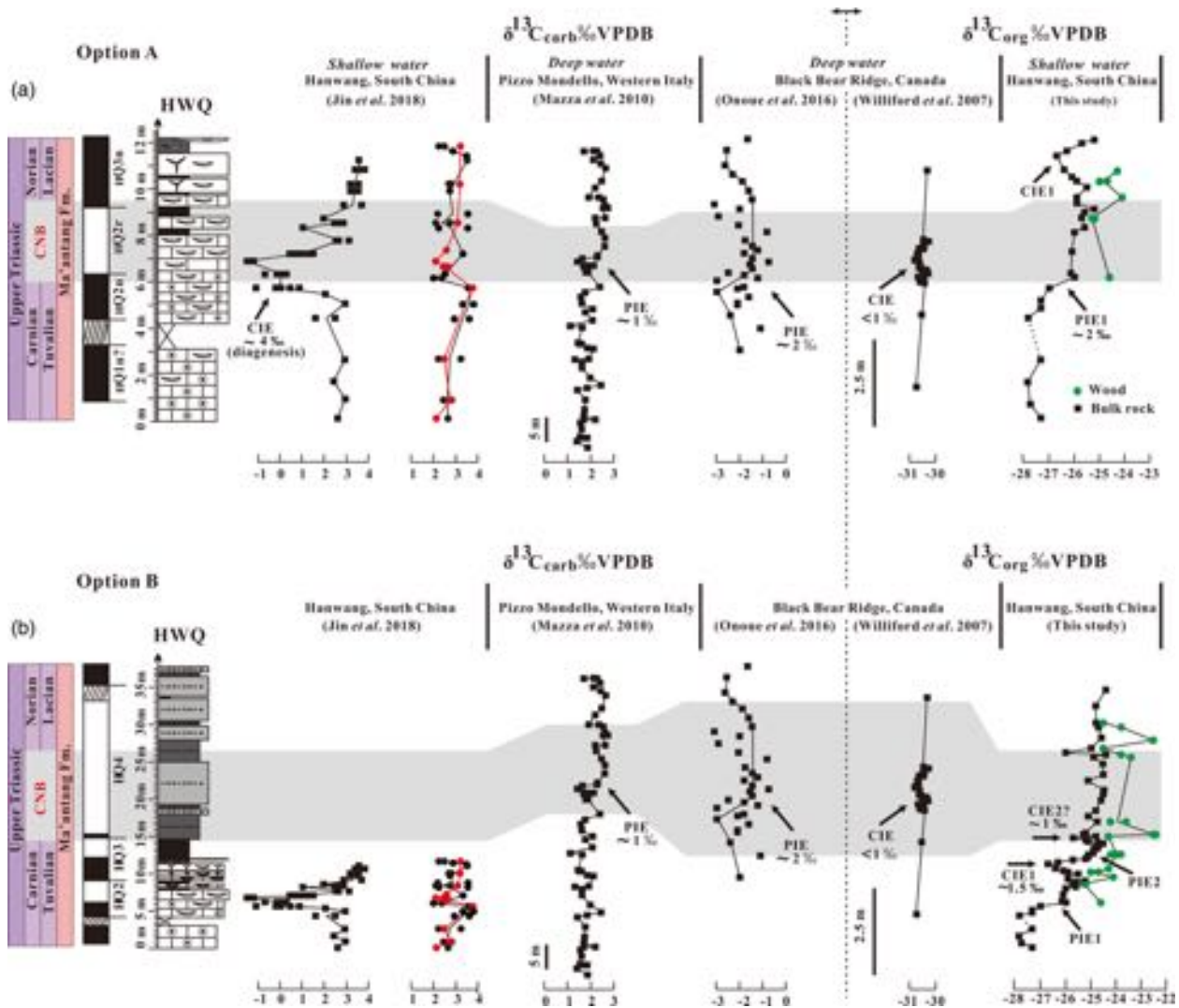
Fig. 11. Comparison of carbon isotope (organic and carbonate) records from the HWQ section, South China and other selected Carnian–Norian boundary (CNB) sections, according to the two correlation options proposed in Figs 9 and 10. In option A, the grey band is the CNB interval according to Mazza *et al.* (2012); that is, between the FO of *Metapolygnathus parvus*, below, and the FO of *Carnepigondolella gulloe* (close to the FO of *Halobia austriaca*), above. For option B, the grey band is the CNB interval according to ammonoid biostratigraphy. At Pizzo Mondello, this interval is between the last occurrence of *Anatropites* sp., below, and the FO of *Dimorphites* spp., above (Balini *et al.* 2012). At Black Bear Ridge, we drawn the CNB interval between the last occurrence of *Anatropites* sp., below, and the FO of *Guembelites jandianus*, above (Orchard 2014).

Wood fragments from the HWQ and JS sections have more positive $\delta^{13}C_{org}$ than marine OM (Fig. 8), within a wide range from −25.35 to −22.07‰. Although wood from the Dolomites has a slightly more positive $\delta^{13}C_{org}$ (Dal Corso *et al.* 2011), this could be ascribed to an undetected difference in taxonomic composition. Triassic land plants were C3 plants, and today C3 plants have an average $\delta^{13}C_{org}$ of *c.* −26‰. Even though the average $\delta^{13}C_{org}$ in the Longmen Shan area is −24.0‰, slightly more positive than present values, it is still within the range of what would be expected for C3 plants (Gröcke 2002; Badeck *et al.* 2005, and references therein). The wide range of $\delta^{13}C_{org}$ from wood fragments reflects a natural dispersion that is expected for plants (e.g. Arens *et al.* 2000; Dal Corso *et al.* 2017) and is common in fossil material (e.g. Dal Corso *et al.* 2011). Owing to its intrinsic variability, an erratic trend is observed in the $\delta^{13}C_{org}$ of wood of the HWQ section (Fig. 2).

The mean value of $\delta^{13}C_{org}$ in terrigenous rocks (Unit 4 in Fig. 2) is between those of wood and bulk OM of the limestone units (Fig. 8), albeit closer to the $\delta^{13}C_{org}$ of wood. These foredeep-deposited terrigenous rocks have been suggested to be related to the uplift of Longmen Mountains and other surrounding palaeolands (Yang *et al.* 2008; Liu *et al.* 2009; Shi *et al.* 2015), thus the $\delta^{13}C_{org}$ of bulk organic carbon in this unit may reflect the mixing of C3 plant

material with marine OM. The different OM source with distinctive ranges of $\delta^{13}C_{org}$ value from limestone and terrigenous units may explain PIE2 (Fig. 2).

Differences in organic carbon sources may also explain other minor features of the $\delta^{13}C_{org}$ record that could not be correlated between the three study sections. In the HWQ section, the well-bedded sponge mound layers are inter-reef deposits that correspond to the mound-shaped sponge reefs in the JS and HWG sections (Wu 1989). A slight negative perturbation of *c.* 1.5‰ in magnitude (CIE1 in Fig. 2) is recorded within the inter-reef deposits, which is not, however, reproduced in the other two sections of this study. We suggest that this local isotopic shift may be related to accumulation of marine OM in this inter-reef environment rather than to a regional or global modification of the organic carbon pools.

Is there a carbon isotopic oscillation at the CNB?

In our correlation Option A (Fig. 11a), a strong isotopic excursion of $\delta^{13}C_{carb}$ nearly coincides with the CNB. However, $\delta^{13}C_{carb}$ from carefully chosen brachiopod shells shows no detectable excursion. This has been explained as the result of early diagenesis of carbonate sediments rich in organic carbon during shallow burial (Jin *et al.*
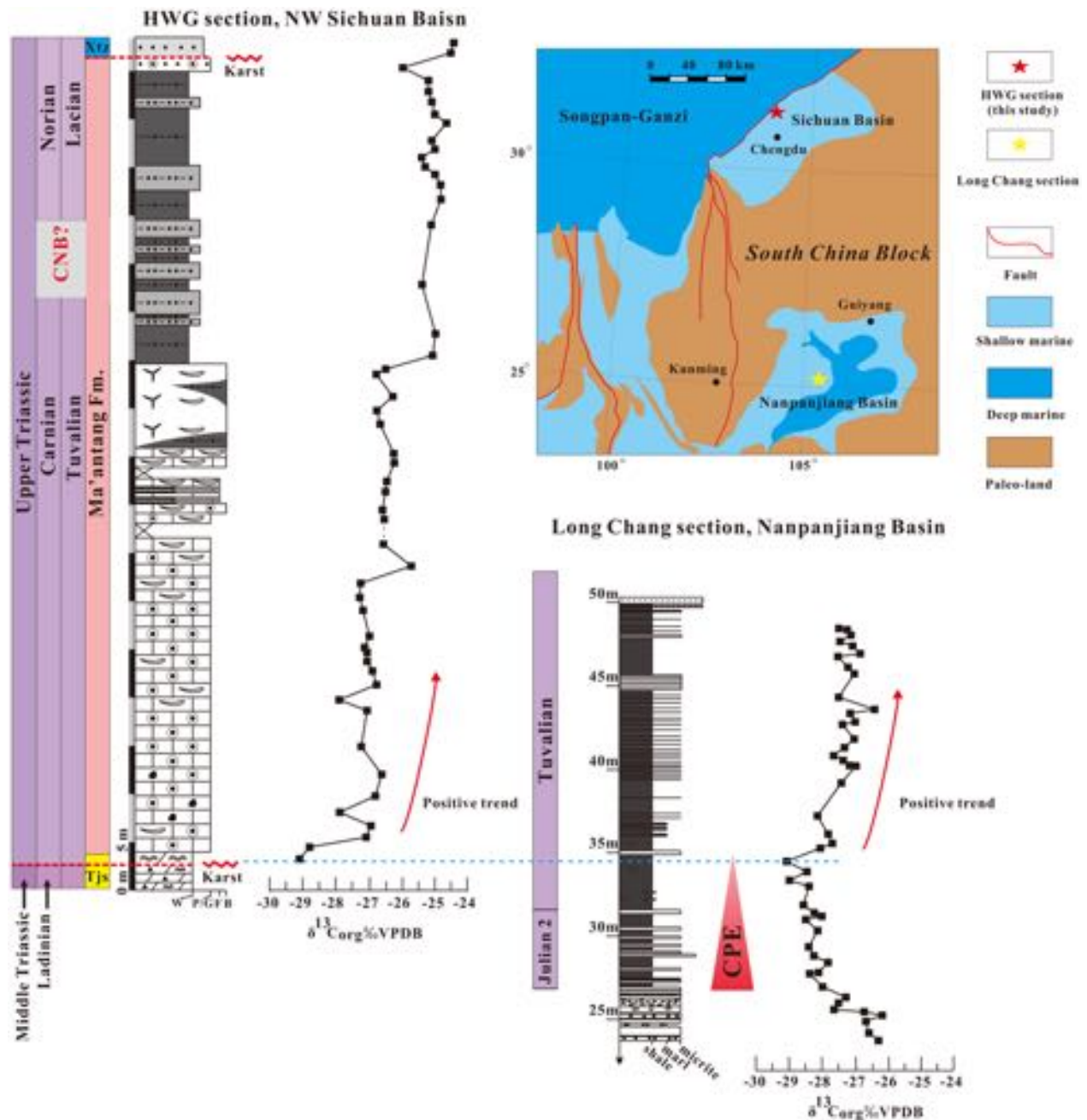
Fig. 12. Comparison of the $\delta^{13}C_{org}$ records between the HWG section, NW Sichuan Basin and Long Chang section, Nanpanjiang Basin (Sun *et al.* 2016). The lower part of the Long Chang section was truncated. The Carnian palaeogeographical map of South China (top right corner) is modified from Ma *et al.* (2009). CPE, Carnian Pluvial Episode.

2018). The $\delta^{13}C_{carb}$ record from brachiopods is considered to represent a more pristine record of seawater $\delta^{13}C$ than bulk carbonate (Brand 1989; Brand *et al.* 2003; Korte *et al.* 2005). Although a 1‰ magnitude shift is still found in brachiopod data near the CNB (Fig. 11a), this may actually derive from the natural range of isotopic variability of brachiopod shells (Korte *et al.* 2017). A PIE in the $\delta^{13}C_{carb}$ across the CNB interval has been reported in many locations (Black Bear Ridge, Onoue *et al.* 2016; Guri Zi, Muttoni *et al.* 2014; Pizzo Mondello, Muttoni *et al.* 2004; Mazza *et al.* 2010; Wadi Mayhah, Sun *et al.* 2018) (only the BBR and PMS sections are displayed in Fig. 11a). This PIE has different shapes and magnitudes and has been reported only from a deep-water setting (Fig. 11a). We could not confirm the occurrence of this PIE at the CNB on the basis of our $\delta^{13}C_{carb}$ data from well-preserved brachiopods.

The $\delta^{13}C_{org}$ records of wood and bulk organic carbon reported in the present paper from the Hanwang and Jushui areas are the first

from the CNB interval in South China. The only counterpart with detailed biostratigraphy is Black Bear Ridge, Canada (Williford *et al.* 2007). A small negative isotopic perturbation, *c.* 0.5‰ in magnitude, was found at the proposed position of the CNB at Black Bear Ridge and was discussed in relation to a fossil turnover observed in the section (Williford *et al.* 2007). In our correlation Option A (Fig. 11a), an opposite shift (PIE1) to more positive values *c.* 2‰ in magnitude occurs in the $\delta^{13}C_{org}$ across the CNB, which is part of a general positive trend within the limestone unit, reproduced in all study sections (Fig. 2).

According to correlation Option B (Fig. 11b), a minor negative shift (CIE2) of *c.* 1‰ is observed at 15 m, at the base of the CNB interval, which is difficult to correlate with Black Bear Ridge because biostratigraphic constraints in this part are poor. Moreover, this negative shift is found in an interval of facies transition characterized by the increase in terrigenous input and therefore

might be related to the mixing of OM from continental and marine sources. As a consequence, the general flat trend of $\delta^{13}C_{org}$ values within the CNB interval (Fig. 11b, grey band) could have recorded a mixed-carbon stable isotopic composition, and the real signal of $\delta^{13}C_{org}$ across the CNB, which could have been masked in our sections.

The end of the Carnian Pluvial Episode in the northwestern Sichuan Basin

The most negative values of $\delta^{13}C_{org}$ are recorded in the lowest part of the HWG section, followed by a long-lasting positive trend (Fig. 2). As this trend is detected within the limestone units (Units 1–3), we assume that the OM source was not changing too much in this interval. The $\delta^{13}C_{org}$ values of limestones in the Sichuan Basin overlap with those during the fading phase of the CPE from the adjacent Nanpanjiang Basin (Fig. 8). We tentatively correlate the carbon isotope records between these two areas (Fig. 12).

The biostratigraphy of the HWG section is still incomplete. The lower Ma'antang Formation yielding most negative $\delta^{13}C_{org}$ values might correspond to approximately the 34 m level in the Long Chang section of Sun *et al.* (2016) and thus to the fading phase of the carbon isotopic excursion (CIE) of the Carnian Pluvial Episode. This trend was recognized clearly in the Ma'antang section, northwestern Sichuan Basin (Shi *et al.* 2018), and it is identifiable in the basal part of our three sections (Fig. 2). The distinctive CIE was also reported in other parts of Tethys (Dal Corso *et al.* 2012, 2015, 2018; Mueller *et al.* 2015, 2016; Miller *et al.* 2017; Baranyi *et al.* 2018; Sun *et al.* 2018) and it is partly missing at the HWG section because it corresponds to a hiatus marked by the basal karstic surface (Figs 2 and 12), which has been interpreted as the forebulge unconformity of the Longmen Shan foreland basin (Li *et al.* 2003, 2011*a*). In the eastern Sichuan Basin, the whole Tianjinshan Formation and the overlying Ma'antang Formation were eroded or were never deposited (Li *et al.* 2003; Mei & Liu 2017).

Conclusions

New biostratigraphic data from the Carnian and Norian of the northwestern Sichuan Basin are provided in this paper. On the basis of an existing magnetostratigraphy and new biostratigraphic age determinations, two possible correlations between the Astrochronostratigraphic Polarity Time Scale of the Triassic and the magnetostratigraphy of the HWQ section are proposed, but further biostratigraphic investigations are needed to identify a preferred correlation. In Option A correlation, the CNB is located between 6 and 9.5 m. In Option B correlation, the CNB could be positioned between 14.5 and 26.5 m of the HWQ section. Furthermore, the occurrence of Carnian conodonts at the base of the JS section implies that some stromatolitic dolostones–limestones in the Sichuan Basin are Carnian rather than Ladinian.

Carbon stable isotopes from wood and bulk organic matter are here measured for the first time in eastern Tethys near the CNB. The recorded variability of $\delta^{13}C_{org}$ between different lithologies is explained by varying organic matter sources. A long-lasting positive trend has been recognized within a uniformly calcareous interval, which can be attributed to the slow recovery from the isotopic perturbations of the CPE and can be correlated with the isotopic record of the Nanpanjiang Basin of South China. Instead, the isotopic record of the CPE in the western Tethys and continental Europe is more complex, featuring repeated negative isotopic excursions, and its correlation with the Sichuan Basin is still uncertain.

Overall, our findings identify the northwestern Sichuan Basin as a relevant area for the study of the CNB. In particular, Carnian–Norian ammonoids, conodonts and bivalves from the Sichuan Basin

are from a much more easterly position than other successions so far considered for the definition of the CNB. These new biostratigraphic data may thus prove useful for a better-informed placement of the Norian GSSP.

References

Anawar, H.M., Yoshioka, T., Konohira, E., Akai, J., Freitas, M.C. & Tareq, S.M. 2010. Sources of organic carbon and depositional environment in the Bengal delta plain sediments during the Holocene period. *Limnology*, **11**, 133–142, https://doi.org/10.1007/s10201-009-0301-9

Arens, N.C., Jahren, A.H. & Amundson, R. 2000. Can C3 plants faithfully record the carbon isotopic composition of atmospheric dioxide? *Paleobiology*, **26**, 137–164, https://doi.org/10.1666/0094-8373(2000)026<0137:CCPFRT>2.0.CO;2

Badeck, F.W., Tcherkez, G., Nogues, S., Piel, C. & Ghashghaie, J. 2005. Post-photosynthetic fractionation of stable carbon isotopes between plant organs – a widespread phenomenon. *Rapid Communications in Mass Spectrometry*, **19**, 1381–1391, https://doi.org/10.1002/rcm.1912

Balini, M., Krystyn, L., Levera, M. & Tripodo, A. 2012. Late Carnian–Early Norian ammonoids from the GSSP candidate section Pizzo Mondello (Sicani Mountains, Sicily). *Rivista Italiana di Paleontologia e Stratigrafia*, **118**, 47–84, https://doi.org/10.13130/2039-4942/5992

Baranyi, V., Miller, C.S., Ruffell, A., Hounslow, M.W. & Kürschner, W.M. 2018. A continental record of the Carnian Pluvial Episode (CPE) from the Mercia Mudstone Group (UK): palynology and climatic implications. *Journal of the Geological Society, London*, https://doi.org/10.1144/jgs2017-150

Brand, U. 1989. Biogeochemistry of Late Paleozoic North American brachiopods and secular variation of seawater composition. *Biogeochemistry*, **7**, 159–193, https://doi.org/10.1007/BF00004216

Brand, U., Logan, A., Hiller, N. & Richardson, J. 2003. Geochemistry of modern brachiopods: applications and implications for oceanography and paleoceanography. *Chemical Geology*, **198**, 305–334, https://doi.org/10.1016/S0009-2541(03)00032-9

Chen, J.h. & Ba, D.Z. 1986. *Halobia* fauna from Zedang of South Xizang with a discussion on the *Halobia* assemblages in China. *Acta Palaeontologica Sinica*, **25**, 1–9.

Cohen, K.M., Finney, S.C., Gibbard, P.L. & Fan, J.X. 2013. The ICS International Chronostratigraphic Chart. *Episodes*, **36**, 199–204.

Dal Corso, J., Preto, N., Kustatscher, E., Mietto, P., Roghi, G. & Jenkyns, H.C. 2011. Carbon isotope variability of Triassic amber, as compared with wood and leaves (Southern Alps, Italy). *Palaeogeography, Palaeoclimatology, Palaeoecology*, **302**, 187–193, https://doi.org/10.1016/j.palaeo.2011.01.007

Dal Corso, J., Mietto, P., Newton, R.J., Pancost, R.D., Preto, N., Roghi, G. & Wignall, P.B. 2012. Discovery of a major negative ^{13}C spike in the Carnian (Late Triassic) linked to the eruption of Wrangellia flood basalts. *Geology*, **40**, 79–82, https://doi.org/10.1130/G32473.1

Dal Corso, J., Gianolla, P. *et al.* 2015. Carbon isotope records reveal synchronicity between carbon cycle perturbation and the 'Carnian Pluvial Event' in the Tethys realm (Late Triassic). *Global and Planetary Change*, **127**, 79–90, https://doi.org/10.1016/j.gloplacha.2015.01.013

Dal Corso, J., Schmidt, A.R. *et al.* 2017. Evaluating the use of amber in palaeoatmospheric reconstructions: The carbon-isotope variability of modern and Cretaceous conifer resins. *Geochimica et Cosmochimica Acta*, **199**, 351–369, https://doi.org/10.1016/j.gca.2016.11.025

Dal Corso, J., Gianolla, P. *et al.* 2018. Multiple negative carbon-isotope excursions during the Carnian Pluvial Episode (Late Triassic). *Earth-Science Reviews*, **185**, 732–750, https://doi.org/10.1016/j.earscirev.2018.07.004.

Deng, K.L., He, L., Qin, D.Y. & He, Z.G. 1982. The earlier late Triassic sequence and its sedimentary environment in western Sichuan basin. *Oil and Gas Geology*, **3**, 204–210 [in Chinese with English abstract].

Enos, P. 1991. Sedimentary parameters for computer modeling. *In*: Franseen, E.K., Watney, W.L., Kendall, C.G.St.C. & Ross, W. (eds) *Sedimentary Modelling*. Kansas Geological Survey Bulletin, **233**, 63–99.

Fogel, M. & Cifuentes, L. 1993. Isotope fractionation during primary production. *In*: Engel, M. & Macko, S. (eds) *Organic Geochemistry: Principles and Applications*. Plenum Press, New York, 73–98.

Fry, B., Scalan, R.S. & Parker, P.L. 1977. Stable carbon isotope evidence for two sources of organic matter in coastal sediments: seagrasses and plankton. *Geochimica et Cosmochimica Acta*, **41**, 1875–1877, https://doi.org/10.1016/0016-7037(77)90218-6

Furin, S., Preto, N., Rigo, M., Roghi, G., Gianolla, P., Crowley, J.L. & Bowring, S.A. 2006. High-precision U–Pb zircon age from the Triassic of Italy: Implications for the Triassic time scale and the Carnian origin of calcareous nannoplankton and dinosaurs. *Geology*, **34**, 1009, https://doi.org/10.1130/G22967A.1

Golonka, J. 2007. Late Triassic and early Jurassic palaeogeography of the world. *Palaeogeography, Palaeoclimatology, Palaeoecology*, **244**, 297–307.

Goñi, M., Ruttenberg, K. & Eglinton, T. 1997. Sources and contribution of terrigenous organic carbon to surface sediments in the Gulf of Mexico. *Nature*, **389**, 275–278, https://doi.org/10.1038/38477

Gou, Z. 1998. The bivalve faunas from the Upper Triassic Xujiahe Formation in the Sichuan Basin. *Sedimentary Facies Palaeogeography*, **18**, 20–31 [in Chinese with English abstract].

Gröcke, D.R. 2002. The carbon isotope composition of ancient CO_2 based on higher-plant organic matter. *Philosophical Transactions of the Royal Society of London, Series A*, **360**, 633–658, https://doi.org/10.1098/rsta.2001.0965

Hayes, J.M., Strauss, H. & Kaufman, A.J. 1999. The abundance of ^{13}C in marine organic matter and isotopic fractionation in the global biogeochemical cycle of carbon during the past 800 Ma. *Chemical Geology*, **161**, 103–125, https://doi.org/10.1016/S0009-2541(99)00083-2

He, L., Li, M., Xiong, L., Ran, F. & Liao, Z. 2011. Re-discussion on the sequence division schemes of Upper Triassic formations in the Sichuan basin. *Natural Gas Industry*, **31**, 28–33 [in Chinese with English abstract].

He, Y. 1980. Sketch of the Triassic foraminiferal biostratigraphy of northwestern Sichuan (Szechuan), China. *Rivista Italiana di Paleontologia e Stratigrafia*, **85**, 1167–1174.

Hesselbo, S.P., Robinson, S.A., Surlyk, F. & Piasecki, S. 2002. Terrestrial and marine extinction at the Triassic–Jurassic boundary synchronized with major carbon-cycle perturbation: A link to initiation of massive volcanism? *Geology*, **30**, 251–254, https://doi.org/10.1130/0091-7613(2002)030<0251:TAMEAT>2.0.CO;2

Jin, X., Ji, G.F., Shi, Z.Q. & Wang, Y.Y. 2015. The sedimentary facies of Guanyinya Section in Hanwang, Mianzhu: implications for the environment evolution ahead of and after the Triassic Carnian Pluvial Event. *Geological Science and Technology Information*, **34**, 1174–1182 [in Chinese with English abstract].

Jin, X., Shi, Z.Q., Rigo, M., Franceschi, M. & Preto, N. 2018. Carbonate platform crisis in the Carnian (Late Triassic) of Hanwang (Sichuan Basin, South China): insights from conodonts and stable isotope data. *Journal of Asian Earth Sciences*, **164**, 104–124, https://doi.org/10.1016/j.jseaes.2018.06.021

Kent, D.V., Olsen, P.E. & Muttoni, G. 2017. Astrochronostratigraphic polarity time scale (APTS) for the Late Triassic and Early Jurassic from continental sediments and correlation with standard marine data. *Earth-Science Reviews*, **166**, 153–180, https://doi.org/10.1016/j.earscirev.2016.12.014

Korte, C., Kozur, H.W. & Veizer, J. 2005. δ^{13}C and δ^{18}O values of Triassic brachiopods and carbonate rocks as proxies for coeval seawater and palaeotemperature. *Palaeogeography, Palaeoclimatology, Palaeoecology*, **226**, 287–306, https://doi.org/10.1016/j.palaeo.2005.05.018

Korte, C., Thibault, N. *et al.* 2017. Brachiopod biogeochemistry and isotope stratigraphy from the Rhaetian Eiberg section in Austria: potentials and limitations. *Neues Jahrbuch für Geologie und Paläontologie, Abhandlungen*, **284**, 117–138, https://doi.org/10.1127/njgpa/2017/0651

Kozur, H. 2003. Integrated ammonoid, conodont and radiolarian zonation of the Triassic. *Hallesches Jahrbuch der Geowissenschaften*, **25**, 49–79.

Krystyn, L. 1982. Obertriassische Ammonoideen aus dem zentralnepalesischen Himalaya (Gebiet von Jomsom). *Abhandlungen der Geologischen Bundesanstalt in Wien*, **36**, 1–63.

Levera, M. 2012. The halobiids from the Norian GSSP candidate section of Pizzo Mondello (Western Sicily, Italy): systematics and correlations. *Rivista Italiana di Paleontologia e Stratigrafia*, **18**, 3–45, https://doi.org/10.13130/2039-4942/5991

Li, L.Q. & Wang, Y.D. 2016. Late Triassic palynofloras in the Sichuan Basin, South China: Synthesis and perspective. *Palaeoworld*, **25**, 212–238, https://doi.org/10.1016/j.palwor.2015.11.009

Li, L.Q., Wang, Y., Liu, Z., Zhou, N. & Wang, Y. 2016. Late Triassic palaeoclimate and palaeoecosystem variations inferred by palynological record in the northeastern Sichuan Basin, China. *PalZ*, **90**, 327–348, https://doi.org/10.1007/s12542-016-0309-5

Li, L.Q., Wang, Y., Vajda, V. & Liu, Z. 2017a. Late Triassic ecosystem variations inferred by palynological records from Hechuan, southern Sichuan Basin, China. *Geological Magazine*, 1–18, https://doi.org/10.1017/S0016756817000735

Li, M., Zhang, Y. *et al.* 2017b. Astronomical tuning and magnetostratigraphy of the Upper Triassic Xujiahe Formation of South China and Newark Supergroup of North America: implications for the Late Triassic time scale. *Earth and Planetary Science Letters*, **475**, 207–223, https://doi.org/10.1016/j.epsl.2017.07.015

Li, Y., Allen, P.A., Densmore, A.L. & Qiang, X. 2003. Evolution of the Longmen Shan foreland basin (western Sichuan, China) during the Late Triassic Indosinian orogeny. *Basin Research*, **15**, 117–138, https://doi.org/10.1046/j.1365-2117.2003.00197.x

Li, Y., Su, D.C., Dong, S.L., Yan, Z.K., He, P. & Yan, L. 2011a. The recognition of the basal unconformity in the Longmenshan foreland basin: Transition from passive continent margin to foreland basin. *Acta Petrologica Sinica*, **27**, 2413–2422 [in Chinese with English abstract].

Li, Y., Sun, D.C. *et al.* 2011b. Dynamic of drowning of the carbonate ramp and sponge build-up in the early stage (Carnian) of Longmen Shan foreland basin, Late Triassic, China. *Acta Petrologica Sinica*, **27**, 3460–3470 [in Chinese with English abstract].

Li, Y., Yan, Z. *et al.* 2014. Migration of the carbonate ramp and sponge buildup driven by the orogenic wedge advance in the early stage (Carnian) of the Longmen Shan foreland basin, China. *Tectonophysics*, **619**, 179–193, https://doi.org/10.1016/j.tecto.2013.11.011

Liu, S.G., Tong, Z.G., Luo, Z.L., Dai, S.L., Pang, J.L., Zhang, G.Z. & He, L. 1995. The formation and evolution of Late Triassic foreland basin in West Sichuan. *Natural Gas Industry*, **15**, 11–15 [in Chinese with English abstract].

Liu, S.G., Yang, R.J., Wu, X.C., Sun, W. & Chen, Y. 2009. The Late Triassic transition from marine carbonate rock to clastics in the western Sichuan Basin. *Oil and Gas Geology*, **30**, 556–566 [in Chinese with English abstract].

Lucas, S.G. 2018. The Late Triassic Timescale. *In*: Tanner, L.H. (ed.) *The Late Triassic World: Earth in a Time of Transition*. Springer, Cham, 1–25.

Ma, Q.H., Chen, J.H., Lan, X., Gu, Z.W., Chen, C.C. & Lin, M.J. 1976. Triassic Lamellibranchia. *In*: Nanjing Institute of Geology and Palaeontology & Academia Sinica (eds) *Mesozoic Lamellibranchia of Yunnan, Mesozoic Fossils of Yunnan, Volume A*. Science Press, Beijing, 161–386 [in Chinese].

Ma, Y., Chen, H. & Wang, G. 2009. *Atlas of Tectonics and Sequence Lithofacies Palaeogeography in South China from Sinian to Neogene*. Science Press, Beijing, 1–301 [in Chinese].

Mazza, M., Furin, S., Spötl, C. & Rigo, M. 2010. Generic turnovers of Carnian/Norian conodonts: Climatic control or competition? *Palaeogeography, Palaeoclimatology, Palaeoecology*, **290**, 120–137, https://doi.org/10.1016/j.palaeo.2009.07.006

Mazza, M., Rigo, M. & Gullo, M. 2012. Taxonomy and biostratigraphic record of the Upper Triassic conodonts of the Pizzo Mondello section (western Sicily, Italy), GSSP candidate for the base of the Norian. *Rivista Italiana di Paleontologia e Stratigrafia*, **118**, 85–130, https://doi.org/10.13130/2039-4942/5993

Mazza, M., Nicora, A. & Rigo, M. 2018. *Metapolygnathus parvus* Kozur, 1972 (Conodonta): a potential primary marker for the Norian GSSP (Upper Triassic). *Bollettino della Società Paleontologica Italiana*, **57**, 81–101, https://doi.org/10.4435/BSPI.2018.06

McArthur, J.M., Tyson, R.V., Thomson, J. & Mattey, D. 1992. Early diagenesis of marine organic matter: Alteration of the carbon isotopic composition. *Marine Geology*, **105**, 51–61, https://doi.org/10.1016/0025-3227(92)90181-G

McRoberts, C.A. 2007. The halobiid bivalve succession across a potential Carnian/Norian GSSP at Black Bear Ridge, Williston Lake, northeast British Columbia, Canada. *Albertiana*, **36**, 142–145.

McRoberts, C.A. 2010. Biochronology of Triassic bivalves. *In*: Lucas, S.G. (ed.) *The Triassic Time Scale*. Geological Society, London, Special Publications, **334**, 201–219, https://doi.org/10.1144/SP334.9

McRoberts, C.A. 2011. Late Triassic Bivalvia (chiefly Halobiidae and Monotidae) from the Pardonet Formation, Williston Lake area, northeast British Columbia, Canada. *Journal of Paleontology*, **85**, 615–666, https://doi.org/10.1666/10-051.1

Mei, M. & Liu, S. 2017. The Late Triassic Sequence-Stratigraphic Framework of the Upper Yangtze Region, South China. *Acta Geologica Sinica (English Edition)*, **91**, 51–75, https://doi.org/10.1111/1755-6724.13063

Mietto, P., Manfrin, S. *et al.* 2012. The global boundary stratotype section and point (GSSP) of the Carnian stage (Late Triassic) at Prati di Stuores/Stuores Wiesen section (Southern Alps, NE Italy). *Episodes*, **35**, 414.

Miller, C.N. 1982. Current status of Paleozoic and Mesozoic conifers. *Review of Palaeobotany and Palynology*, **37**, 99–114, https://doi.org/10.1016/0034-6667(82)90039-2

Miller, C.S., Peterse, F., da Silva, A.C., Baranyi, V., Reichart, G.J. & Kürschner, W.M. 2017. Astronomical age constraints and extinction mechanisms of the Late Triassic Carnian crisis. *Scientific Reports*, **7**, 2557, https://doi.org/10.1038/s41598-017-02817-7

Mueller, S., Hounslow, M.W. & Kürschner, W.M. 2015. Integrated stratigraphy and palaeoclimate history of the Carnian Pluvial Event in the Boreal realm; new data from the Upper Triassic Kapp Toscana Group in central Spitsbergen (Norway). *Journal of the Geological Society, London*, **173**, 186–202, https://doi.org/10.1144/jgs2015-028

Mueller, S., Krystyn, L. & Kürschner, W.M. 2016. Climate variability during the Carnian Pluvial Phase – A quantitative palynological study of the Carnian sedimentary succession at Lunz am See, Northern Calcareous Alps, Austria. *Palaeogeography, Palaeoclimatology, Palaeoecology*, **441**, 198–211, https://doi.org/10.1016/j.palaeo.2015.06.008

Muttoni, G., Kent, D.V., Di Stefano, P., Gullo, M., Nicora, A., Tait, J. & Lowrie, W. 2001. Magnetostratigraphy and biostratigraphy of the Carnian/Norian boundary interval from the Pizzo Mondello section (Sicani Mountains, Sicily). *Palaeogeography, Palaeoclimatology, Palaeoecology*, **166**, 383–399, https://doi.org/10.1016/S0031-0182(00)00224-8

Muttoni, G., Kent, D.V., Olsen, P.E., Di Stefano, P., Lowrie, W., Bernasconi, S.M. & Hernández, F.M. 2004. Tethyan magnetostratigraphy from Pizzo

Mondello (Sicily) and correlation to the Late Triassic Newark astrochronological polarity time scale. *Geological Society of America Bulletin*, **116**, 1043–1058, https://doi.org/10.1130/B25326.1

Muttoni, G., Mazza, M., Mosher, D., Katz, M.E., Kent, D.V. & Balini, M. 2014. A Middle -Late Triassic (Ladinian -Rhaetian) carbon and oxygen isotope record from the Tethyan Ocean. *Palaeogeography, Palaeoclimatology, Palaeoecology*, **399**, 246–259, https://doi.org/10.1016/j.palaeo.2014.01.018

Nicora, A., Balini, M. *et al.* 2007. The Carnian/Norian boundary interval at Pizzo Mondello (Sicani Mountains, Sicily) and its bearing for the defnition of the GSSP of the Norian Stage. *Albertiana*, **36**, 102–129.

Nordt, L., Tubbs, J. & Dworkin, S. 2016. Stable carbon isotope record of terrestrial organic materials for the last 450 Ma. *Earth-Science Reviews*, **159**, 103–117, https://doi.org/10.1016/j.earscirev.2016.05.007

Onoue, T., Zonneveld, J.P., Orchard, M.J., Yamashita, M., Yamashita, K., Sato, H. & Kusaka, S. 2016. Paleoenvironmental changes across the Carnian/Norian boundary in the Black Bear Ridge section, British Columbia, Canada. *Palaeogeography, Palaeoclimatology, Palaeoecology*, **441**, 721–733, https://doi.org/10.1016/j.palaeo.2015.10.008

Orchard, M.J. 2007. A proposed Carnian–Norian boundary GSSP at Black Bear Ridge, northeast British Columbia, and a new conodont framework for the boundary interval. *Albertiana*, **36**, 130–141.

Orchard, M.J. 2014. Conodonts from the Carnian–Norian boundary (Upper Triassic) of Black Bear Ridge, Northeasern British Columbia, Canada. *New Mexico Museum of Natural History and Science Bulletin*, **64**, 1–139.

Orchard, M.J., McRoberts, C.A., Tozer, E.T., Johns, M.J., Sandy, M.R. & Shaner, J.S. 2001. An intercalibrated biostratigraphy of the Upper Triassic of Black Bear Ridge, Williston Lake, northeast British Columbia. *Geological Survey of Canada, Current Research*, **2001-A6**, 21.

Raup, D.M. & Sepkoski, J.J. 1982. Mass extinctions in the marine fossil record. *Science*, **215**, 1501–1503, https://doi.org/10.1126/science.215.4539.1501

Renner, S.S. 2009. Gymnosperms. *In*: Hedges, S.B. & Kumar, S. (eds) *The Time Tree of Life Book*. Oxford University Press, New York, 157–160.

Rigo, M., Preto, N., Franceschi, M. & Guaiumi, C. 2012. Stratigraphy of the Carnian–Norian Calcari con Selce Formation in the Lagonegro Basin, Southern Apennines. *Rivista Italiana di Paleontologia e Stratigrafia*, **118**, 143–154, https://doi.org/10.13130/2039-4942/5995

Rigo, M., Mazza, M., Karádi, V. & Nicora, A. 2018. New Upper Triassic Conodont Biozonation of the Tethyan Realm. *In*: Tanner, L.H. (ed.) *The Late Triassic World: Earth in a Time of Transition*. Springer, Cham, 189–235.

Roghi, G. 2004. Palynological investigations in the Carnian of the Cave del Prdil area (Julian Alps, NE Italy). *Review of Palaeobotany and Palynology*, **132**, 1–35, https://doi.org/10.1016/j.revpalbo.2004.03.001

Roghi, G., Gianolla, P., Minarelli, L., Pilati, C. & Preto, N. 2010. Palynological correlation of Carnian humid pulses throughout western Tethys. *Palaeogeography, Palaeoclimatology, Palaeoecology*, **290**, 89–106, https://doi.org/10.1016/j.palaeo.2009.11.006

Schoene, B., Guex, J., Bartolini, A., Schaltegger, U. & Blackburn, T.J. 2010. Correlating the end-Triassic mass extinction and flood basalt volcanism at the 100 ka level. *Geology*, **38**, 387–390, https://doi.org/10.1130/G30683.1

Shi, Z.Q., Ou, L., Luo, F., Li, Y. & Qian, L. 2009. Black shale event during the Late Triassic Carnian Age: implications of sedimentary and palaeontological records in Longmen Mountains region. *Journal of Palaeogeography*, **11**, 375–383 [in Chinese with English abstract].

Shi, Z.Q., Preto, N. *et al.* 2017. Demise of Late Triassic sponge mounds along the northwestern margin of the Yangtze Block, South China: Related to the Carnian Pluvial Phase? *Palaeogeography, Palaeoclimatology, Palaeoecology*, **474**, 247–263, https://doi.org/10.1016/j.palaeo.2016.10.031

Shi, Z.Q., Jin, X., Preto, N., Rigo, M., Du, Y.X. & Han, L. 2018. The Carnian Pluvial Episode at Ma'antang, Jiangyou in Upper Yangtze Block, Southwestern China. *Journal of the Geological Society, London*, https://doi.org/10.1144/jgs2018-038

Shi, Z.S., Wang, Z.H., Hao, C.G., Guo, C.M. & Mo, W.L. 2015. Sedimentary facies of the Upper Triassic Ma'antang Formation in Sichuan Basin. *Journal of Palaeogeography*, **17**, 772–786 [in Chinese with English abstract].

Silberling, N.J. & Tozer, E.T. 1968. *Biostratigraphic Classification of the Marine Triassic in North America*. Geological Society of America, Special Papers, **110**, https://doi.org/10.1130/SPE110-p1

Simms, M.J. & Ruffell, A.H. 1989. Synchroneity of climatic change and extinctions in the Late Triassic. *Geology*, **17**, 265–268, https://doi.org/10.1130/0091-7613(1989)017<0265:SOCCAE>2.3.CO;2

Simms, M.J. & Ruffell, A.H. 2018. The Carnian Pluvial Episode: From discovery, through obscurity, to acceptance. *Journal of the Geological Society, London*, **175**, 989–992, https://doi.org/10.1144/jgs2018-020

Sun, Y.D., Wignall, P.B. *et al.* 2016. Climate warming, euxinia and carbon isotope perturbations during the Carnian (Triassic) Crisis in South China. *Earth and Planetary Science Letters*, **444**, 88–100, https://doi.org/10.1016/j.epsl.2016.03.037

Sun, Y.D., Richoz, S., Krystyn, L., Zhang, Z. & Joachimski, M. 2018. Perturbations in carbon cycle during the Carian Humid Episode: Carbonate carbon isotope records from southwestern China and northern Oman. *Journal of the Geological Society, London*, https://doi.org/10.1144/jgs2017-170

Tozer, E.T. 1994. *Canadian Triassic Ammonoid Faunas*. Geological Survey of Canada Bulletin, **467**.

Wang, Y.S. 1992. The earlier late Triassic ammonites from Longmen Mountains. *Journal of Chengdu College of Geology*, **19**, 28–35 [in Chinese with English abstract].

Wang, Q., Zhang, Y. & Wu, X. 2015. Triassic (Carnian) hexactinellid–thrombolite reef mounds and oolitic bank complex in NW Sichuan, China. *Carbonates and Evaporites*, **30**, 187–205, https://doi.org/10.1007/s13146-014-0203-8

Wang, Z.H. & Dai, J.Y. 1981. Triassic conodonts from the Jiangyou–Beichuan area, Sichuan province. *Acta Palaeontologica Sinica*, **20**, 138–152 [in Chinese with English abstract].

Wendt, J. 2001. Upper Triassic (Carnian) mud mounds from northern Sichuan (China). *Acta Geologica Polonica*, **51**, 1–13.

Whiteside, J.H., Olsen, P.E., Eglinton, T., Brookfield, M.E. & Sambrotto, R.N. 2010. Compound-specific carbon isotopes from Earth's largest flood basalt eruptions directly linked to the end-Triassic mass extinction. *Proceedings of the National Academy of Sciences of the USA*, **107**, 6721–6725, https://doi.org/10.1073/pnas.1001706107

Williford, K.H., Orchard, M.J., Zonneveld, J.P., McRoberts, C. & Beatty, T.W. 2007. A record of stable organic carbon isotopes from the Carnian–Norian boundary section at Black Bear Ridge, Williston Lake, British Columbia, Canada. *Albertiana*, **36**, 146–148.

Wu, X. 1984. Paleoecological characteristics of Late Triassic sponge patch reefs in northwestern Sichuan. China. *Journal of Chengdu College of Geology*, **1**, 43–54 [in Chinese with English abstract].

Wu, X. 1989. Carnian (upper Triassic) sponge mounds of the Northwestern Sichuan Basin, China: Stratigraphy, facies and paleoecology. *Facies*, **21**, 171–187, https://doi.org/10.1007/BF02536835

Wu, X. 2009. Sedimentary facies analysis of the Late Triassic Carnian siliceous sponge reef–oolitic bank complex in northwestern Sichuan province. *Journal of Palaeogeography*, **11**, 125–142 [in Chinese with English abstract].

Yang, R.J., Liu, S.G., Wu, X.C., Zhao, X.F., Peng, J.S. & Sun, W. 2008. Distribution characteristics and controlling factors of Upper Triassic Ma'antang Formation in the front of Longmen Mountains, Sichuan, China. *Journal of Chengdu University of Technology (Science & Technology Edition)*, **38**, 455–462 [in Chinese with English abstract].

Zhang, B., Wang, Z.J., Shi, Z.Q., Cheng, M., Duan, X., Jin, X. & Cui, L. 2013. Discovery and geological significance of unconformity surface between Upper Triassic Ma'antang formation and Xiaotangzi formation in Hanwang of Mianzhu in Northwest Sichuan, China. *Journal of Chengdu University of Technology (Science & Technology Edition)*, **40**, 80–88 [in Chinese with English abstract].

Zhang, G., Meng, Q., Yu, Z., Sun, Y., Zhou, D. & Guo, A. 1996. Orogenesis and dynamics of the Qinling orogen. *Science in China Series D, Earth Sciences*, **39**, 225–234 [in Chinese with English abstract].

Zhang, Y., Li, M.S. *et al.* 2015. Cycle-calibrated magnetostratigraphy of middle Carnian from south China: implications for Late Triassic time scale and termination of the Yangtze platform. *Palaeogeography, Palaeoclimatology, Palaeoecology*, **436**, 135–166, https://doi.org/10.1016/j.palaeo.2015.05.033

Zhang, Z.M., Chen, C.Z. & Wen, S.X. 1985. Fossil lamellibranchs from Eastern Xizang, Western Sichuan and Western Yunnan. *In*: Nanjing Institute of Geology and Palaeontology & Academia Sinica (eds) *Stratigraphy and Palaeontology in Western Sichuan, Western Xizang, China, Part 3, Regional Geological Survey of Sichuan Bureau of Geology*. People's Publishing House of Sichuan, Chengdu, 25–150 [in Chinese].

Zonneveld, J.P., Beatty, T.W., Williford, K.H., Orchard, M.J. & McRoberts, C.A. 2010. Stratigraphy and sedimentology of the lower Black Bear Ridge section, British Columbia: candidate for the base-Norian GSSP. *Stratigraphy*, **7**, 61–82.